

1 Full Title: **Cyfp2 controls the acoustic startle threshold through FMRP, actin**

2 **polymerization, and GABA<sub>B</sub> receptor function.**

3 Short Title: **Cyfp2 controls startle sensitivity via FMRP, Rac1 and GABA<sub>B</sub> receptors.**

4

5 Jacob C. Deslauriers<sup>1</sup>, Rohit P. Ghotkar<sup>1,3</sup>, Lindsey A. Russ<sup>1,4</sup>, Jordan A. Jarman<sup>1,5</sup>, Rubia M.

6 Martin<sup>1,6</sup>, Rachel G. Tippet<sup>1</sup>, Sureni H. Sumathipala<sup>1</sup>, Derek F. Burton<sup>1,7</sup>, D. Chris Cole<sup>1</sup>, Kurt C.

7 Marsden<sup>\*1,2</sup>

8 1. Department of Biological Sciences, North Carolina State University, Raleigh, North  
9 Carolina, USA

10 2. Center for Human Health and the Environment (CHHE), North Carolina State University,  
11 Raleigh, North Carolina, USA

12 3. Current address: Putnam Associates, Boston, Massachusetts, USA

13 4. Current address: Department of Pharmacology & Physiology, Georgetown University,  
14 Washington D.C., USA

15 5. Current address: Department of Physiology and Biophysics, Boston University, Boston,  
16 MA, USA

17 6. Current address: U.S. Environmental Protection Agency, Raleigh-Durham-Chapel Hill,  
18 North Carolina, USA

19 7. Current address: Biogen, Durham, North Carolina, USA

20 \*Corresponding author: [kcmarsde@ncsu.edu](mailto:kcmarsde@ncsu.edu)

21

22 **Author contributions:** Conceptualization: JCD and KCM; Data curation: JCD, RAM; Formal  
23 analysis: JCD, RAM, RGT, SHS, DCC, KCM; Funding acquisition: KCM; Investigation: JCD,  
24 RPG, LAR, JAJ, RAM, RGT, SHS, DFB, DCC, KCM; Methodology: JCD, RAM, KCM; Project  
25 administration: KCM; Supervision: JCD, DFB, DCC, KCM; Visualization: JCD, RAM, KCM;  
26 Writing – original draft: JCD; Writing – review and editing: JCD, KCM

27 **Abstract**

28           Animals process a constant stream of sensory input, and to survive they must detect and  
29 respond to dangerous stimuli while ignoring innocuous or irrelevant ones. Behavioral responses  
30 are elicited when certain properties of a stimulus such as its intensity or size reach a critical  
31 value, and such behavioral thresholds can be a simple and effective mechanism to filter sensory  
32 information. For example, the acoustic startle response is a conserved and stereotyped  
33 defensive behavior induced by sudden loud sounds, but dysregulation of the threshold to initiate  
34 this behavior can result in startle hypersensitivity that is associated with sensory processing  
35 disorders including schizophrenia and autism. Through a previous forward genetic screen for  
36 regulators of the startle threshold a nonsense mutation in *Cytoplasmic Fragile X Messenger*  
37 *Ribonucleoprotein (FMRP)-interacting protein 2 (cyfip2)* was found that causes startle  
38 hypersensitivity in zebrafish larvae, but the molecular mechanisms by which Cyfip2 establishes  
39 the acoustic startle threshold are unknown. Here we used conditional transgenic rescue and  
40 CRISPR/Cas9 to determine that Cyfip2 acts through both Rac1 and FMRP pathways, but not the  
41 closely related FXR1 or FXR2, to establish the acoustic startle threshold during early  
42 neurodevelopment. To identify proteins and pathways that may be downstream effectors of  
43 Rac1 and FMRP, we performed a candidate-based drug screen that indicated that Cyfip2 can  
44 also act acutely to maintain the startle threshold branched actin polymerization and N-methyl D-  
45 aspartate receptors (NMDARs). To complement this approach, we used unbiased discovery  
46 proteomics to determine that loss of Cyfip2 alters cytoskeletal and extracellular matrix  
47 components while also disrupting oxidative phosphorylation and GABA receptor signaling.  
48 Finally, we functionally validated our proteomics findings by showing that activating GABA<sub>B</sub>  
49 receptors, which like NMDARs are also FMRP targets, restores normal startle sensitivity in  
50 *cyfip2* mutants. Together, these data reveal multiple mechanisms by which Cyfip2 regulates  
51 excitatory/inhibitory balance in the startle circuit to control the processing of acoustic  
52 information.

## 53 **Introduction**

54           To navigate their environments to find food and avoid predation, animals must be able to  
55 filter out extraneous stimuli but respond appropriately to salient ones, a process known as  
56 sensorimotor gating. Specific attributes of a stimulus can trigger a response; for visual stimuli  
57 the luminance, size, and speed of the stimulus determine if escape and reorientation responses  
58 are initiated [1–3]. Similarly, the intensity and frequency of acoustic stimuli determine whether a  
59 response is made [4,5]. One way in which animals can control their responses to sensory stimuli  
60 is by establishing a behavioral threshold such that when one or more of these stimulus  
61 attributes reaches a critical value a specific behavioral response is initiated. Behavioral  
62 thresholds are a fundamental mechanism of sensorimotor gating used across the animal  
63 kingdom to regulate a wide range of behavioral responses including both collective responses,  
64 such as fanning behaviors for hive climate regulation in bees [6,7] and shoaling behavior in fish  
65 [8,9], as well as individual responses to odors [10–13], tactile stimuli [14–17], changes in  
66 luminance and contrast of visual stimuli [1,18–21], and sound frequency and intensity in  
67 mammals and fish [5,22–24]. That behavioral over-responsiveness to visual, tactile, and  
68 acoustic stimuli is observed across a number of neuropsychiatric conditions including autism,  
69 anxiety, and schizophrenia [4,22,24–28] highlights the importance of setting such behavioral  
70 thresholds at an appropriate level. Yet our knowledge of the molecular mechanisms that both  
71 establish and maintain behavioral thresholds is limited.

72           Previously, to identify genes that regulate the threshold for initiating the acoustic startle  
73 response, a highly conserved behavior initiated following sudden loud sounds that may indicate  
74 danger [5,29–31], we conducted a standard 3-generation, ENU-based forward genetic screen in  
75 larval zebrafish [32]. We identified a set of five mutant lines that display acoustic startle  
76 hypersensitivity, and through whole-genome sequencing of the *triggerhappy* mutant line, we  
77 identified a causal, nonsense mutation in *cytoplasmic Fragile X Messenger Ribonucleoprotein*  
78 (*FMRP*)-*Interacting protein 2 (cyfip2)*. *Cyfip2* was first identified as an interactor of FMRP and

79 the elongation initiation factor 4E (eIF4E), through which it participates in translational  
80 repression of many target transcripts [33,34]. Cyfip2, but not the closely related Cyfip1, can also  
81 bind the Fragile X-related proteins FXR1 and FXR2, but the function of these interactions is  
82 unknown [33]. Additionally, Cyfip2 interacts with the activated form of the small Rho GTPase  
83 Rac1, and it is a member of the WAVE Regulatory Complex (WRC) in which it helps regulate  
84 Arp2/3 activation and branched actin polymerization [35–41]. Cyfip2 is vital for proper neuronal  
85 migration and cell movement, axonal growth and guidance, as well as synapse formation and  
86 function in flies, mice, and zebrafish [32,33,37,42–47]. Homozygous *cyfip2* mutations are  
87 embryonically lethal in mammals and fatal after 7-8 days post-fertilization (dpf) in zebrafish  
88 [32,42,44,48]. Despite its key role in multiple aspects of neurodevelopment, the links between  
89 how Cyfip2 regulates RNA translation, actin polymerization, and behavior have not been  
90 defined. Our previous work demonstrated that loss of Cyfip2 causes acoustic startle  
91 hypersensitivity that is reversible upon transgenic expression of GFP-tagged Cyfip2, alters the  
92 morphology but not the electrophysiological properties of the startle command-like Mauthner  
93 cells (M-cells), and causes hyperexcitability of the spiral fiber neurons (SFNs), a set of hindbrain  
94 excitatory interneurons that project to the M-cell axon hillock [32]. It is unclear, however,  
95 whether Cyfip2 acts via Rac1-mediated actin polymerization or through FMRP-mediated  
96 translational repression to control the startle threshold. Furthermore, the downstream molecular  
97 changes that directly modulate the function of the startle circuit have not been identified.

98         In this study we used an inducible rescue approach in *cyfip2* mutant zebrafish larvae to  
99 demonstrate that both Cyfip2's Rac1 and FMRP interactions are required for establishing the  
100 acoustic startle threshold during early neurodevelopment. Using CRISPR-Cas9 gene  
101 knockdown we find that FXR1 and FXR2 are dispensable for startle regulation and that Cyfip2  
102 acts through FMRP. Furthermore, with a candidate-based pharmacological approach we show  
103 that Cyfip2 mediates Arp2/3-induced branched actin polymerization and may modulate N-  
104 methyl-D-aspartate receptors (NMDARs) to alter neuronal function in the acoustic startle circuit.

105 Finally, we performed discovery proteomics to define molecular pathways disrupted by loss of  
106 *Cyfp2* *in vivo*. Our results indicate roles for *Cyfp2* in mitochondrial function, oxidative  
107 phosphorylation, and inhibitory Gamma-Aminobutyric Acid (GABA) receptor signaling. We  
108 confirmed the functional importance of this last finding using the GABA<sub>B</sub> receptor agonist  
109 baclofen, which rescues *cyfp2* mutants' hypersensitivity. Together these data establish a novel  
110 pathway that links *Cyfp2*, actin dynamics, RNA translation, and excitatory/inhibitory balance in  
111 the control of acoustic responsiveness.

112

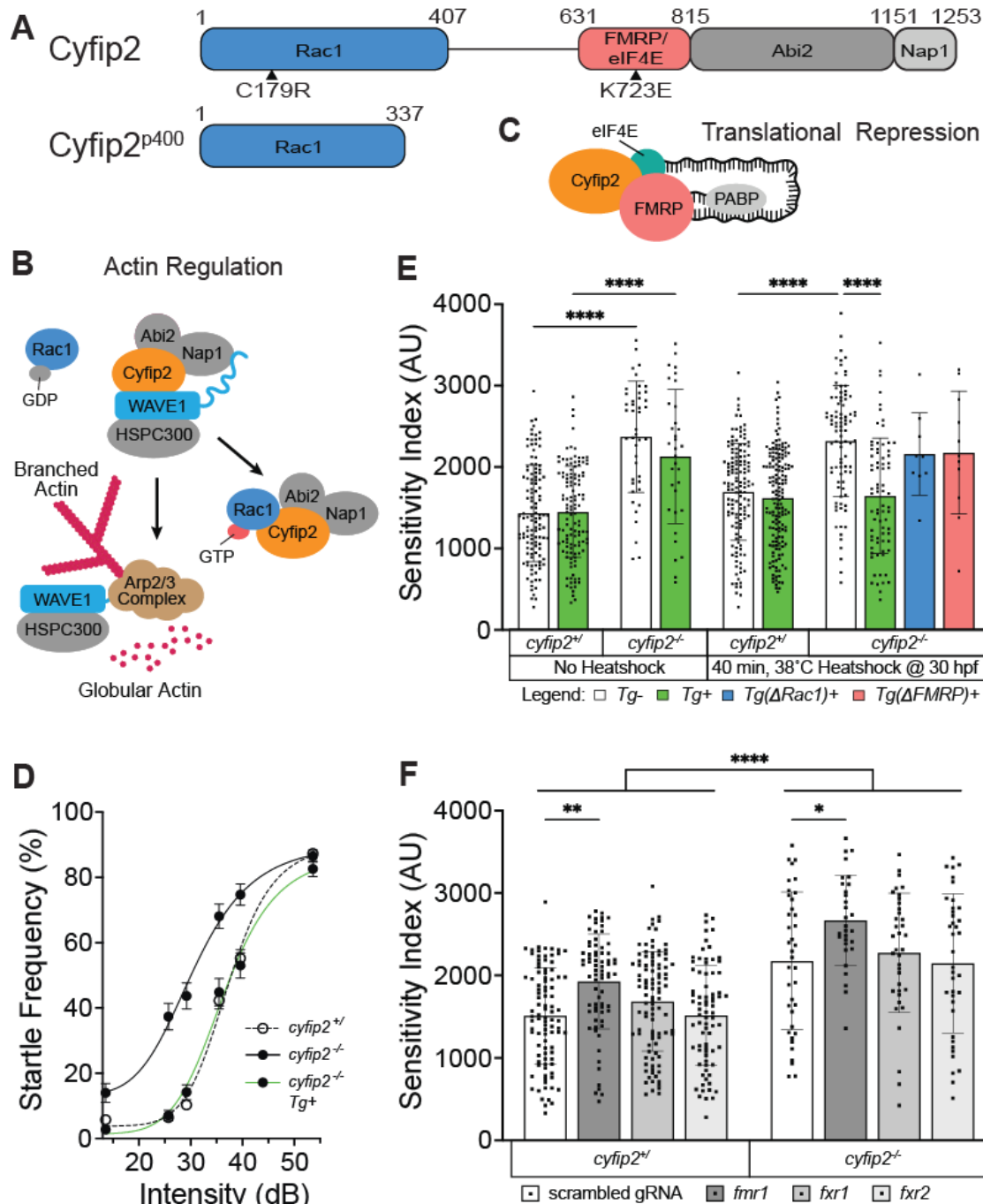
## 113 Results

114 *Cyfp2* establishes the acoustic startle threshold through both *Rac1* and *FMRP* during early  
115 neurodevelopment.

116 *Cyfp2* has four known protein-interaction domains [49] (Fig. 1A), and it can act through  
117 *Rac1* to promote actin polymerization (Fig. 1B) and *FMRP* to regulate RNA translation (Fig. 1C).  
118 *cyfp2*<sup>p400</sup> mutants have a single base pair transversion (nt1024; T to A) resulting in a premature  
119 stop codon at amino acid position 343 (Fig. 1A) [32]. *cyfp2*<sup>p400</sup> mutant zebrafish larvae (5 dpf)  
120 were previously shown to display acoustic startle hypersensitivity that could be rescued by  
121 expressing *Cyfp2* at 30 hours post fertilization (hpf) using a stable heatshock-inducible  
122 transgenic line, *Tg(hsp70:cyfp2-EGFP)* [32]. We replicate those findings here, using a 60-  
123 stimulus assay consisting of 10 trials at each of 6 intensities with a 20 second (s) interstimulus  
124 interval (ISI) to measure startle sensitivity (Fig. 1D). A 40-min heatshock at 30 hpf restores  
125 normal sensitivity in transgenic (*Tg+*) but not in non-transgenic (*Tg-*) *cyfp2* mutants (Fig. 1D,E).  
126 Previous studies have established that C179R and K723E amino acid substitutions prevent  
127 *Cyfp2* from binding with *Rac1* and *FMRP*, respectively [34,39,45]. To determine if *Cyfp2*  
128 engages *Rac1*-mediated actin regulation and/or *FMRP*/eIF4E-mediated translational repression  
129 pathways to establish the acoustic startle threshold, we induced C179R ( $\Delta$ *Rac1*) and K723E  
130 ( $\Delta$ *FMRP*) point mutations in the *Tg(hsp70:cyfp2-EGFP)* construct and created stable transgenic

131 lines for each (Fig. 1A). We expressed either wildtype or mutant ( $\Delta Rac1$ ;  $\Delta FMRP$ ) versions of  
132 Cyfip2 in mutants at 30 hpf with a 40-minute heatshock at 38°C, followed by acoustic startle  
133 testing at 5 dpf. While expression of wildtype *Tg(hsp70:cyfip2-EGFP)* at 30 hpf rescues mutant  
134 hypersensitivity, expression of  $\Delta Rac1$  or  $\Delta FMRP$  versions of Cyfip2 in mutants was insufficient  
135 to rescue mutant hypersensitivity (Fig. 1E).

136 *cyfip2* mutants also display a number of kinematic defects in their performance of the  
137 startle response [32]. To determine if Rac1 and FMRP binding are also required for Cyfip2 to  
138 regulate startle kinematics, we analyzed startle latency, duration, head turn angle (C1 angle),  
139 and total distance traveled during the response in *Tg-* and *Tg+* fish after the same 40-min  
140 heatshock protocol at 30 hpf (Fig. S1). Heatshock induction of wildtype Cyfip2 restored normal  
141 latency, duration, and C1 angle, but not distance traveled (Fig. S1). All kinematic defects  
142 remained in *cyfip2* mutant larvae expressing  $\Delta Rac1$ -Cyfip2 (Fig. S1), but expression of  $\Delta FMRP$ -  
143 Cyfip2 was sufficient to rescue startle duration and induced a trend toward rescue of startle  
144 latency and C1 turn angle (Fig. S1). These data suggest that Rac1 binding is required for all  
145 aspects of Cyfip2-mediated startle regulation, while FMRP binding is required to regulate the  
146 startle threshold but is largely dispensable for startle kinematics.



147  
 148 **Figure 1. Cyfip2 establishes the acoustic startle threshold through Rac1 and FMRP.** (A) Cyfip2  
 149 protein interacting domain diagram of wildtype (top) and mutant (bottom) Cyfip2 proteins. Black  
 150 arrowheads indicate the positions of induced mutations in Cyfip2, eliminating the Rac1- (C179R) or  
 151 FMRP/eIF4E (K723E)-binding capacity of Cyfip2. (B) Cyfip2 actin regulatory pathway wherein Cyfip2  
 152 (orange) upon stimulation by Rac1-GTP triggers WAVE1 activation, Arp2/3-complex initiation and  
 153 branched actin nucleation. (C) Cyfip2 translational repression pathway in which Cyfip2, eIF4E (teal), and  
 154 FMRP (pink) along with the poly-A binding protein (PABP; gray), sequester neurodevelopmentally  
 155 important mRNAs from being translated. (D) Average startle frequency (%) after 10 trials at 13.6, 25.7,  
 156 29.2, 35.5, 39.6 and 53.6 dB for 5 dpf *cyfip2* siblings (+/-) and mutant (-/-) larvae heatshocked at 30 hpf for  
 157 40 minutes at 38°C. The average startle frequency curve for *cyfip2* siblings (+/-; open circles, dashed line),  
 158 *cyfip2* mutants (-/-; closed circles, solid line) and *cyfip2* mutants harboring the *Tg(hsp70:cyfip2-EGFP)*<sup>+</sup>  
 159 transgene (-/-; *Tg*<sup>+</sup>; closed circles, solid green line). (E) Sensitivity indices, calculated as the area under

160 the startle frequency curves, for 5 dpf *cyfip2* siblings and mutants, following a 40-minute heatshock at 30  
161 hpf to express either wildtype (*Tg+*; green), *Rac1-* ( $\Delta$ *Rac1+*; blue) or FMRP/eIF4E- ( $\Delta$ *FMRP+*; pink)  
162 binding deficient versions of *Cyfip2*-EGFP. Comparisons were made to both non-transgenic (*Tg-*) and  
163 non-heatshocked controls. All indices (mean  $\pm$  SD) compared using a Kruskal-Wallis test with Dunn's  
164 multiple comparisons correction;  $p^{****} < 0.0001$ . (F) Sensitivity indices for 5 dpf *cyfip2* sibling (+/) and  
165 mutant (-/-) larvae following 1-cell stage injection with CRISPR-Cas9 and a single, *scrambled* guide RNA  
166 (gRNA) or dual gRNA cocktails targeting *fmr1*, *fxr1*, or *fxr2*. *scrambled* gRNA injected (white bar, closed  
167 circles); *fmr1* gRNA injected (dark gray bar closed circles); *fxr1* gRNA injected (medium gray bar; closed  
168 circles); *fxr2* gRNA injected (light gray bar, closed circles). Comparisons were made both within genotype  
169 and between genotypes by condition. All indices (mean  $\pm$  SD) compared using an Ordinary one-way  
170 ANOVA with Sidak's multiple comparisons correction;  $p^* < 0.05$ ;  $p^{**} < 0.01$ ;  $p^{****} < 0.0001$ .  
171

172 One possible explanation for these results is that expression levels may differ between  
173 the three heatshock transgenic lines. We therefore measured expression levels of each  
174 transgenic *Cyfip2*-GFP protein 6 hours after a 40-min heatshock by fluorescence intensity (Fig.  
175 S2A). The  $\Delta$ *Rac1* and  $\Delta$ *FMRP* lines displayed GFP expression that was not significantly  
176 different than the wildtype *Tg+* line but which trended lower. To induce expression of wildtype  
177 *Cyfip2*-GFP at levels more comparable to the  $\Delta$ *Rac1* and  $\Delta$ *FMRP* lines after 40-minute  
178 heatshock, we delivered a 15-min heatshock at 30 hpf in the wildtype *Tg+* line. The 15-min  
179 heatshock reduced peak *Cyfip2*-GFP expression to levels comparable to or below that of the  
180  $\Delta$ *Rac1* and  $\Delta$ *FMRP* lines, and this level of expression was also sufficient to rescue acoustic  
181 startle sensitivity in *cyfip2* mutants (Fig. S2A-C). Thus, the level of transgene expression cannot  
182 account for the failure of the  $\Delta$ *Rac1* and  $\Delta$ *FMRP* constructs to rescue startle phenotypes, and  
183 these findings support our conclusion that *Cyfip2* utilizes both *Rac1*- and FMRP-mediated  
184 pathways to establish the acoustic startle threshold.

185

186 *Cyfip2* acts through FMRP but not FXR1/2 to establish the acoustic startle threshold.

187 We previously found that FMRP is not required to establish a normal startle threshold, as  
188 *fmr1*<sup>hu2787</sup> mutants' startle sensitivity is unaffected [32]. Having established that the K723 residue  
189 that *Cyfip2* uses to bind FMRP is required for normal startle sensitivity, however, we  
190 hypothesized that *Cyfip2* may instead interact with other members of the Fragile X protein  
191 family, Fragile X-related proteins 1 and 2 (FXR1/2), to establish the acoustic startle threshold



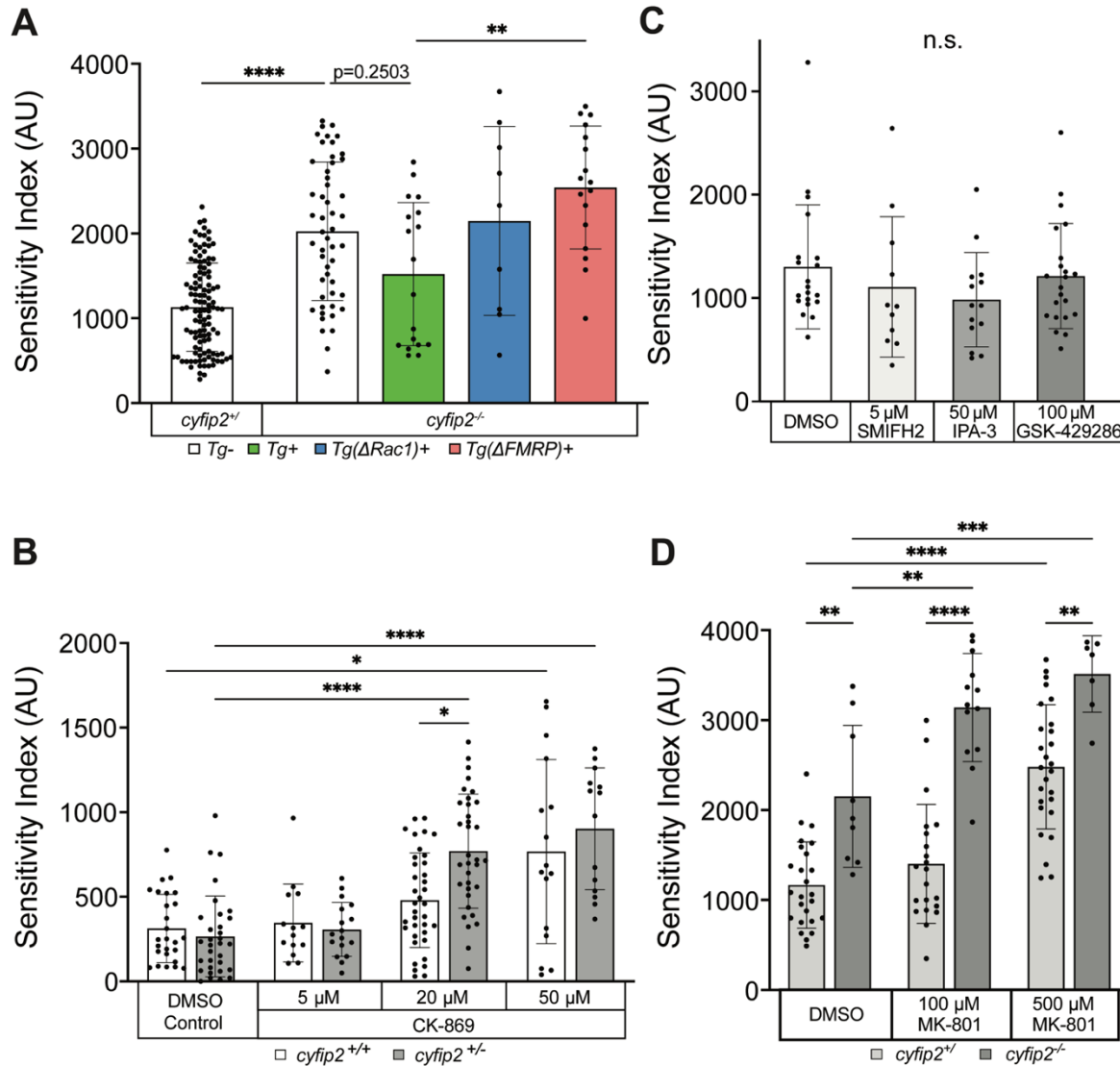
192 [33]. We designed pairs of CRISPR guide RNAs (gRNAs) targeting each of the *fmr1*, *fxr1* and  
193 *fxr2* genes. We injected *fmr1*-, *fxr1*- or *fxr2*-specific CRISPR-Cas9 cocktails into 1-cell stage  
194 *cyfip2* sibling and mutant embryos and measured acoustic startle sensitivity in these crispant  
195 larvae at 5 dpf (Fig. 1F). Highly efficient CRISPR-induced mutagenesis was observed for all 3  
196 genes, with 4 of the 6 gRNAs inducing edits as confirmed by PCR amplification and Sanger  
197 sequencing (Fig. S3A-F). Quantitative PCR confirmed that mRNA expression of all three genes  
198 was strongly reduced by CRISPR/Cas9 injection (Fig. S3G). FMRP crispants had significantly  
199 increased startle sensitivity compared to larvae injected with a scrambled gRNA plus Cas9, and  
200 sensitivity of FMRP crispants was even further increased in the *cyfip2* mutant background (Fig.  
201 1F). However, startle sensitivity was unaltered in FXR1 or FXR2 crispants in either *cyfip2*  
202 siblings or mutants (Fig. 1F). These data indicate that FMRP, but not FXR1/2, regulates the  
203 startle threshold. The discrepancy between our hypersensitive *fmr1* crispants and prior analysis  
204 of non-hypersensitive *fmr1*<sup>hu2787</sup> mutants could be due to genomic adaptation that has been  
205 reported in the *fmr1*<sup>hu2787</sup> mutant line that may partially compensate for the loss of FMRP [50]. In  
206 support of this, an independently created CRISPR-generated *fmr1* mutant line displayed  
207 additional behavioral and developmental phenotypes not originally seen in the *fmr1*<sup>hu2787</sup> line  
208 [51]. *fmr1*<sup>hu2787</sup> mutant larvae have been found to express other autism-related phenotypes,  
209 however, such as altered social behavior and preference for reduced sensory stimulation [52],  
210 as well as increased brain activity in response to acoustic stimulation [53]. Together our  
211 conditional rescue and *fmr1* crispant data provide clear evidence that Cyfip2 acts in part through  
212 FMRP to establish the acoustic startle threshold.

213

214 Cyfip2 can acutely maintain the acoustic startle threshold through Rac1 and FMRP pathways.

215 Our previous study found that Cyfip2 is important for both establishing the acoustic  
216 startle threshold during early neurodevelopment, and for actively modulating the threshold later  
217 in development between 4 and 6 dpf [32]. Here we sought to define a critical window for Cyfip2

218 expression in regulating the startle threshold using our heatshock transgenic lines. Our results  
219 show that while a 40-minute heatshock to induce expression of wildtype *Cyfip2* (*Tg+*) at 30 hpf  
220 is sufficient for behavioral rescue in 5 dpf *cyfip2* mutant larvae (Fig. 1D,E), a 40-min heatshock  
221 at 2, 3, or 4 dpf fails to rescue *cyfip2* mutant hypersensitivity (Fig. S4). Heatshock-induced  
222 expression at 5 dpf, 4 hours prior to testing, resulted in a trend toward rescue and a bi-modal  
223 distribution with some *cyfip2* mutants remaining hypersensitive and a second population  
224 showing restoration of normal sensitivity (Fig. 2A). These results are similar to our prior findings  
225 [32], and they suggest that *Cyfip2* can not only function during the development of the startle  
226 circuit but can also actively maintain the circuit's threshold after it has formed. Next, to  
227 determine if *Cyfip2* employs both of its canonical pathways in maintaining the startle threshold  
228 after 4 dpf, we expressed either  $\Delta Rac1$  or  $\Delta FMRP$  versions of *Cyfip2* in *cyfip2* mutants at 5 dpf  
229 with a 40-min heatshock followed by acoustic startle behavior testing 6 hours later. Similar to  
230 what we observed with the developmental heatshock (Fig. 1E), neither expression of the  $\Delta Rac1$   
231 nor the  $\Delta FMRP$  version of *Cyfip2* at 5 dpf rescued acoustic hypersensitivity of *cyfip2* mutants  
232 (Fig 2A). These findings suggest that *Cyfip2* uses both its Rac1- and FMRP-mediated pathways  
233 to both establish and dynamically maintain the acoustic startle threshold throughout  
234 neurodevelopment.



235

236 **Figure 2. Cyfip2 acutely regulates branched actin polymerization and NMDARs to establish the**  
 237 **acoustic startle threshold.** (A) Sensitivity indices for 5 dpf *cyfip2* sibling (+/) and mutant (-/) larvae,  
 238 following a 40-minute heatshock at 120 hpf (5 dpf) to express either wildtype (*Tg*<sup>+</sup>; green), Rac1-  
 239 ( $\Delta$ Rac1<sup>+</sup>; blue) or FMRP/eIF4E- ( $\Delta$ FMRP<sup>+</sup>; pink) binding deficient versions of Cyfip2-EGFP. Comparisons  
 240 were made to non-transgenic (*Tg*<sup>-</sup>), heatshocked sibling (+) and mutant (-) controls. All indices (mean  $\pm$   
 241 SD) compared using a Kruskal-Wallis test with Dunn's multiple comparisons correction; p-values listed;  
 242 p<sup>\*\*</sup> < 0.01, p<sup>\*\*\*\*</sup> < 0.0001. (B) Sensitivity indices for 5 dpf *cyfip2* wildtype (+/+; white bar) and  
 243 heterozygous (+/-; gray bar) larvae, treated for 30 minutes on d5 with 5, 20 or 50  $\mu$ M CK-869.  
 244 Comparisons were made both within genotype and within condition. All indices (mean  $\pm$  SD) compared  
 245 using a Kruskal-Wallis test with Dunn's multiple comparisons correction; p<sup>\*</sup> < 0.05; p<sup>\*\*\*\*</sup> < 0.0001. (C)  
 246 Sensitivity indices for 5 dpf Tüpfel longfin (TLF) larvae treated for 30 minutes on d5 with the highest, non-  
 247 lethal doses the formin antagonist (SMIFH2; 5  $\mu$ M), PAK3 antagonist (IPA-3; 50  $\mu$ M) and ROCK  
 248 antagonist (GSK429286; 100  $\mu$ M). Comparisons were made between respective treatments and the  
 249 DMSO controls. All indices (mean  $\pm$  SD) were compared using a Kruskal-Wallis test with Dunn's multiple  
 250 comparisons correction; All comparisons made were non-significant (n.s.). (D) Sensitivity indices for 5 dpf  
 251 *cyfip2* sibling (+/) and mutant (-) larvae, treated for 30 minutes on d5 with 100 or 500  $\mu$ M MK-801.  
 252 Comparisons were made both between genotypes within condition and between conditions by genotype.  
 253 All indices (mean  $\pm$  SD) were compared using an Ordinary one-way ANOVA with Tukey's multiple  
 254 comparisons correction. p<sup>\*\*</sup> < 0.01; p<sup>\*\*\*</sup> < 0.001; p<sup>\*\*\*\*</sup> < 0.0001.

255  
256

257 Cyfp2 maintains the acoustic startle threshold through branched actin polymerization.

258           Regulation of the actin cytoskeleton is a vital cellular process that within the context of  
259 the nervous system is critical for cell migration and movement, synapse formation, function and  
260 plasticity, receptor anchoring and trafficking, as well as axon growth and guidance [54]. Given  
261 our findings that Cyfp2 can act through the Rac1-WAVE pathway to establish and modulate the  
262 acoustic startle threshold, we hypothesized that Cyfp2-mediated branched actin polymerization  
263 specifically modulates the startle threshold. To test this hypothesis, we incubated 5 dpf *cyfp2*  
264 heterozygous and wildtype larvae in the Arp2/3 antagonist CK-869 at 5, 20, or 50  $\mu$ M for 30  
265 minutes, followed by acoustic startle testing. In control conditions, *cyfp2* heterozygotes display  
266 startle sensitivity equal to that of wildtypes (Fig. 2B), and incubation at 5  $\mu$ M did not significantly  
267 alter startle sensitivity of either heterozygotes or wildtypes (Fig 2B). At 20  $\mu$ M, wildtype larvae  
268 are unaffected by CK-869, but *cyfp2* heterozygotes have significantly increased startle  
269 sensitivity compared to controls (Fig 2B). 50  $\mu$ M CK-869 caused both *cyfp2* wildtype and  
270 heterozygous larvae to become significantly hypersensitive compared to controls, phenocopying  
271 *cyfp2* mutants. Thus, Arp2/3-mediated, branched actin polymerization is necessary for acutely  
272 maintaining the acoustic startle threshold. That *cyfp2* heterozygotes display hypersensitivity at  
273 20  $\mu$ M but wildtypes do not indicates that a single functional copy of *cyfp2* is insufficient to  
274 maintain normal startle circuit function when branched actin polymerization is limited by a  
275 moderate dose of CK-869. We found similar results when exposing larvae to another Arp2/3  
276 antagonist, CK-666, with both *cyfp2* heterozygotes and wildtypes phenocopying mutant  
277 hypersensitivity at a 50  $\mu$ M concentration (Table S2). These findings support the conclusion that  
278 Cyfp2-dependent Arp2/3-mediated branched actin polymerization is necessary to maintain the  
279 acoustic startle threshold.

280           The actin cytoskeleton is dynamic and requires the action of both branched and  
281 unbranched actin regulatory pathways to maintain cellular structure and function. Unbranched  
282 filamentous (F) actin is polymerized from globular actin monomers by dimeric complexes of  
283 formin proteins, which bind at the barbed ends of new filaments and promote their elongation  
284 [55–58]. Another form of actin regulation involves the action of cofilin, an actin severing protein  
285 that cleaves existing filaments to create new barbed ends and increase the rate of actin turnover  
286 within the cell [59]. To determine whether unbranched actin and severing pathways play a role  
287 in regulating the acoustic startle threshold we incubated 5 dpf wildtype larvae in a formin  
288 antagonist, SMIFH2, or the cofilin disinhibitors, IPA-3 and GSK429286, for 30 minutes followed  
289 by acoustic startle testing. Treatment with 5  $\mu$ M SMIFH2 or with 50  $\mu$ M IPA-3 or 100  $\mu$ M  
290 GSK429286 did not significantly affect startle sensitivity in wildtype larvae (Fig 2C). We also  
291 tested these drugs at higher concentrations, which were lethal after a 30-minute exposure, as  
292 well as longer exposures at lower concentrations, which had no effect on startle sensitivity  
293 (Table S1). Our data with the formin inhibitor SMIFH2 are in contrast to a recent finding showing  
294 that Formin 2B morpholino knockdown caused a decrease in Mauthner cell-mediated fast startle  
295 responses in zebrafish larvae [60]. That we did not observe any change in startle frequency  
296 could be due to the acute nature of our pharmacological approach as opposed to the  
297 morpholino-mediated developmental knockdown of Formin 2B. Our findings suggest that acute  
298 perturbations to unbranched actin filaments and actin turnover do not play a significant role in  
299 regulating the acoustic startle threshold. Altogether, these data further support our conclusion  
300 that Cyfip2-mediated, branched actin polymerization is a key pathway for acutely maintaining  
301 the acoustic startle threshold.

302

303 Cyfip2 may regulate NMDA receptors to modulate the acoustic startle threshold.

304           While we have established that Cyfip2 mediates the establishment and maintenance of  
305 the acoustic startle threshold through both branched actin and FMRP regulatory pathways, it is

306 unclear what molecular mechanisms directly modulate the excitability of the startle circuit. To  
 307 identify molecules that may be downstream effectors of *Cyfp2* in modulating activity of the  
 308 startle circuit, we conducted a candidate-based small-molecule screen with compounds  
 309 previously shown to alter startle sensitivity in wildtype zebrafish larvae (Table 1) [61]. In this  
 310 screen we incubated *cyfp2* wildtype, heterozygous, and mutant larvae in each compound for 30  
 311 min prior to and during acoustic startle testing. Consistent with previous findings, *N*-  
 312 phenylanthranilic acid (NPAA; Cl<sup>-</sup> channel antagonist), Meclofenamic acid (MA; K<sup>+</sup> channel and  
 313 gap junction antagonist), Phenoxybenzamine (POBA; alpha-adrenergic receptor and calmodulin  
 314 antagonist), Etazolate (ETAZ; phosphodiesterase 4 (PDE4) inhibitor), and MK-801 (N-methyl-D-  
 315 aspartate receptor (NMDAR) antagonist) all increased startle sensitivity in a dose-dependent  
 316 manner (Table 1). BMS204352, a different K<sup>+</sup> channel antagonist, did not alter acoustic startle  
 317 sensitivity at either 10 or 50 μM concentrations, and NSC-23766, a Rac1 antagonist, reduced  
 318 sensitivity in siblings at 100 μM, but not *cyfp2* mutants.  
 319

Compound	Concentration (μM)	Effect By Genotype		
		<i>cyfp2</i> (+/+)	<i>cyfp2</i> (+/-)	<i>cyfp2</i> (-/-)
NPAA (Cl <sup>-</sup> channel antagonist)	1	93.21% of Control, p > 0.99	110.21% of Control, p < 0.99	113.57% of Control, p > 0.99
	5	140.11% of Control, p = 0.9785	137.32% of Control, p = 0.1385	140.29% of Control, p > 0.2787
	10	<b>234.14% of Control, p** = 0.0038</b>	<b>201.29% of Control, p**** &lt; 0.0001</b>	<b>155.06% of Control, p* = 0.0189</b>
MA (K <sup>+</sup> channel/gap jxn. antagonist)	1	131.6% of Control, p > 0.99	11.87% of Control, p > 0.99	132.29% of Control, p = 0.5732
	5	137.24% of Control, p > 0.99	138.46% of Control, p = 0.0622	112.29% of Control, p > 0.99
	10	214.13% of Control, p = 0.0833	<b>169.81% of Control, p* = 0.0188</b>	<b>155.76% of Control, p* = 0.0288</b>
POBA (AAR/calmodulin antagonist)	1	102.9% of Control, p > 0.99	107.08% of Control, p > 0.99	101.04% of Control, p > 0.99
	10	136.17% of Control, p > 0.99	106.58% of Control, p > 0.99	99.01% of Control, p > 0.99
	50	<b>175.8% of Control, p* = 0.0123</b>		99.76% of Control, p > 0.99
ETAZ (PDE4 inhibitor)	1	141.79% of Control, p > 0.99	126.36% of Control, p > 0.99	121.74% of Control, p > 0.99
	10	168.6% of Control, p = 0.5472	<b>172.26% of Control, p* = 0.0137</b>	152.73% of Control, p = 0.3977

	50	<b>236.64% of Control, p** = 0.0029</b>	<b>179.99% of Control, p** = 0.0015</b>	<b>149.75% of Control, p* = 0.0105</b>
MK-801 (NMDAR antagonist)	100	120.19% of Control, p > 0.99		<b>145.93% of Control, p** = 0.0024</b>
	500	<b>212.69% of Control, p**** &lt; 0.0001</b>		<b>163.26% of Control, p*** = 0.0002</b>
BMS-204352 (K+ channel antagonist)	10	79.48% of Control, p = 0.4269		89.55% of Control, p > 0.99
	50	76.08% of Control, p = 0.6759		108.74% of Control, p > 0.99
NSC-23766 (Rac1 antagonist)	100	<b>49.14% of Control, p*** = 0.0002</b>		81.60% of Control, p > 0.99
	200	86.26% of Control, p > 0.99		105.28% of Control, p > 0.99

320

321 **Table 1. Cyfip2 may regulate NMDARs to control acoustic startle sensitivity.** Mean startle index  
322 comparisons, listed as percentage (%) of the mean startle index of vehicle-treated controls by *cyfip2*  
323 genotype and drug concentration, for larvae treated with compounds targeting the indicated pathways  
324 [61] to increase acoustic startle sensitivity. All significant differences (p < 0.05) are listed (**bold**) for  
325 comparisons using a Kruskal-Wallis test and Dunn's multiple comparisons correction. NPAA (*N*-  
326 phenylanthranilic acid); MA (meclofenamic acid); POBA (phenoxybenzamine); ETAZ (etazolate).

327 To determine whether any of the targeted pathways may be downstream of *Cyfip2*, we looked  
328 for conditions in which there was a clear *cyfip2* genotype-specific effect on sensitivity. The  
329 NMDA receptor blocker MK-801 showed the clearest such effect, with a low dose (100 μM)  
330 elevating startle sensitivity only in *cyfip2* mutants but not siblings (Table 1). Therefore, *Cyfip2*-  
331 mediated cytoskeletal and/or translational regulation may impact the expression and/or function  
332 of NMDA receptors within the startle circuit to modulate the acoustic startle threshold.

333

334 Proteomic analysis reveals that *Cyfip2*-mediated regulation of GABA<sub>B</sub> receptors is critical for  
335 startle sensitivity.

336 To complement our candidate drug screen with an unbiased approach to identify  
337 proteins and molecular pathways regulated by *Cyfip2*, likely through its role in translational  
338 regulation, we conducted a proteomic analysis of *cyfip2* wildtype, heterozygous, and mutant  
339 larvae at 5 dpf. All larvae used were siblings and were genotyped by PCR and Sanger  
340 sequencing and then pooled in groups of 30 per genotype and snap frozen with liquid nitrogen.  
341 Three independent pools of 30 larvae were analyzed for each genotype. Protein lysates were  
342 submitted to the Molecular Education, Technology and Research Innovation Center (METRIC)

343 at NC State University for protein digestion and LC-MS. Raw LC-MS files were processed and  
344 quantified using MaxQuant (Max Planck Institute of Biochemistry) and imported into Perseus  
345 software for transformation and identification of Differentially Expressed Proteins (DEPs) for  
346 subsequent Ingenuity Pathway Analysis (IPA).

347 Comparative analysis of *cyfip2* heterozygous and mutant versus wildtype proteomes  
348 identified a total of 221 differentially expressed proteins (DEPs) in heterozygotes and 127 DEPs  
349 in mutants (Fig. S5A-B; Tables S7,S8). *Cyfip2* was the most strongly downregulated protein in  
350 mutants, providing a key validation of our unbiased approach (Fig. 3A,S5A; Tables S7,S8).  
351 *Cyfip2* was slightly but significantly downregulated in heterozygotes as well (Fig. S5B), providing  
352 a basis for the sensitization of *Cyfip2* heterozygotes to the actin inhibitor CK-869 (Fig. 2B).  
353 *Cyfip1* expression was not significantly altered in either genotype, indicating that it likely does  
354 not act to compensate for the loss of *Cyfip2* (Fig. S5A-B). 66 DEPs were shared between *cyfip2*  
355 heterozygotes and mutants, while 155 and 61 DEPs were specific to each group, respectively  
356 (Fig. S5C). The top 5 upregulated proteins identified in *cyfip2*<sup>p400</sup> heterozygotes in descending  
357 order included: microtubule actin cross-linking factor 1 (MACF1), acyl-CoA dehydrogenase  
358 family member 11 (ACAD11), cullin 2 (CUL2), calcium channel, voltage dependent, L-type alpha  
359 1S (CACNA1S) and ubiquitin specific peptidase 24 (USP24) (Fig. 3A; top, green). The top 5  
360 downregulated proteins identified in *cyfip2*<sup>p400</sup> heterozygotes in descending order included:  
361 tyrosine 3-monooxygenase/tryptophan 5-monooxygenase activation protein theta or 14-3-3  
362 protein theta (YWHAQ), SEC61 translocon subunit alpha 1 (SEC61A1), ribosomal protein S5  
363 (RPS5), enolase 2 (ENO2), and ribosomal protein L18A (RPL18A) (Fig 3A; top, red). The top 5  
364 upregulated proteins identified in *cyfip2*<sup>p400</sup> mutants in descending order included: ACAD11,  
365 mitochondrial NADH dehydrogenase 4 (MT-ND4), NIPBL cohesion loading factor b (NIPBL),  
366 troponin C2 fast skeletal type (TNNC2), and USP24 (Fig 3A; bottom, green). The top 5  
367 downregulated proteins identified in *cyfip2*<sup>p400</sup> mutants in descending order included:  
368 cytoplasmic FMR1-interacting protein 2 (CYFIP2), collagen type VI alpha 3 (COL6A3), stress-

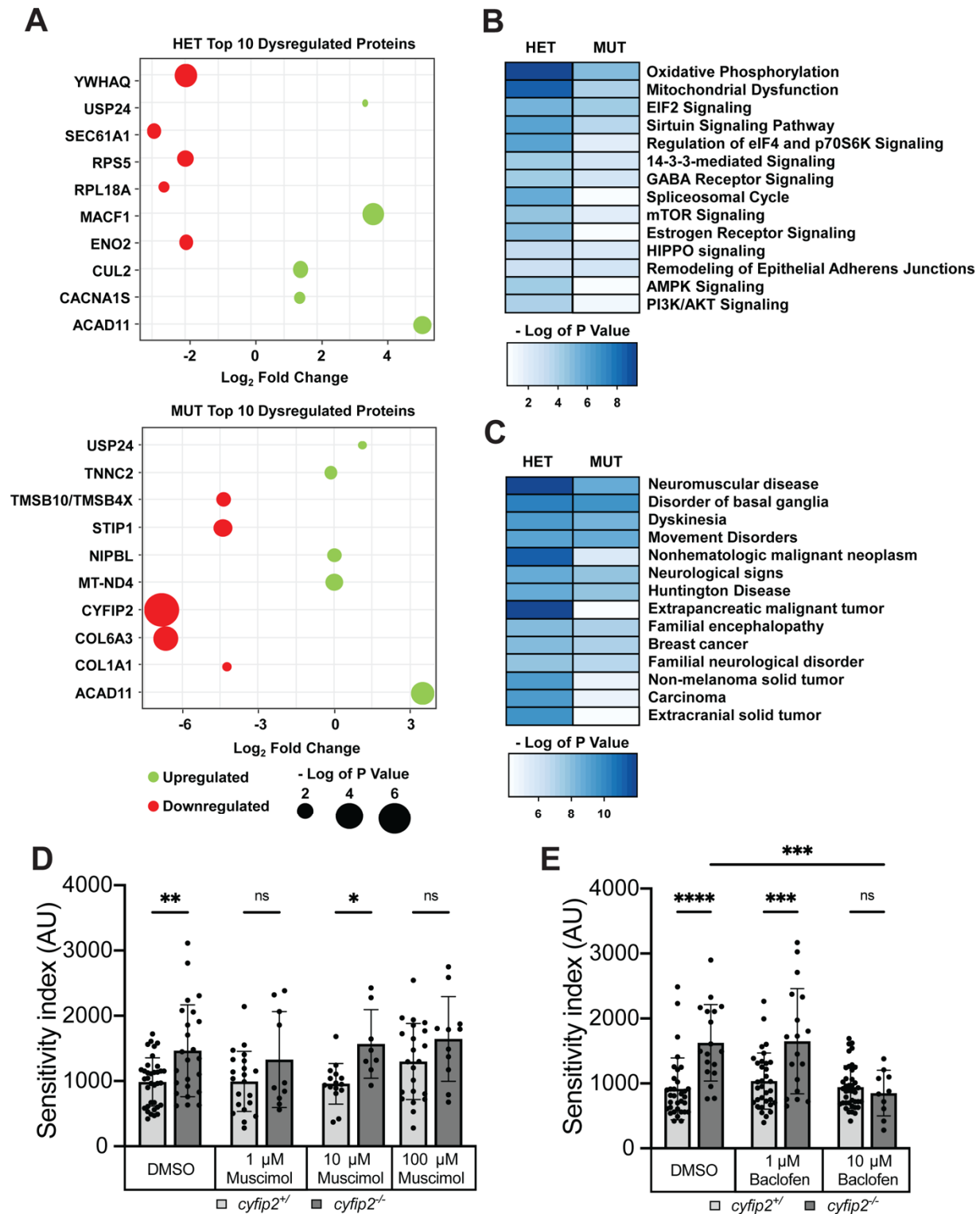


369 induced phosphoprotein 1 (STIP1), thymosin beta (TMSB10/TMSB4X) and collagen type 1  
370 alpha 1 (COL1A1) (Fig 3A; bottom, green). These changes highlight the diverse set of roles that  
371 Cyfip2 plays, impacting translational machinery, metabolism, and the extracellular matrix.

372 IPA analysis of DEPs in *cyfip2* heterozygotes and mutants revealed disruption of  
373 multiple pathways common to both genotypes. Notable disrupted pathways shared between  
374 *cyfip2* heterozygotes and mutants include oxidative phosphorylation, mitochondrial dysfunction,  
375 EIF2 signaling, sirtuin signaling, eIF4/p70S6K signaling, 14-3-3-mediated signaling, and GABA  
376 receptor signaling (Fig. 3B). Analysis of the most affected diseases and functions for each  
377 genotype supports a role for Cyfip2-mediated regulation in neuromuscular disease, disorder of  
378 the basal ganglia, dyskinesia, Huntington disease, breast cancer, familial encephalopathy, and  
379 neurological disorders (Fig. 3C). These data provide further evidence of the central importance  
380 of Cyfip2 for neural function.

381 Finally, we sought to confirm that these pathways play a functional role in regulating  
382 startle sensitivity, and so we focused on GABA receptor signaling as the most likely to  
383 contribute to the hyperexcitability of *cyfip2* mutant larvae. We applied agonists of both ionotropic  
384 GABA<sub>A</sub> receptors (muscimol) and metabotropic GABA<sub>B</sub> receptors (baclofen) for 1 hour prior to  
385 startle testing. Muscimol did not have a consistent impact on mutant hypersensitivity at 1, 10, or  
386 100  $\mu$ M (Fig. 3D), but baclofen induced a clear restoration of normal sensitivity in *cyfip2* mutants  
387 at 10  $\mu$ M (Fig. 3E). Importantly, baclofen application did not cause sedation at this concentration  
388 as mutants were equally responsive as untreated siblings, and the same dose of baclofen did  
389 not affect startle sensitivity in sibling larvae. Thus, Cyfip2 maintains a normal startle threshold by  
390 promoting GABAergic inhibition through the activity of GABA<sub>B</sub> receptors. Together our findings  
391 establish a set of molecular pathways downstream of Cyfip2 that enable the proper processing  
392 of acoustic stimuli to limit sensory over-responsiveness.

393



394

395 **Figure 3. Loss of *Cyfip2* causes widespread proteomic changes and GABA<sub>B</sub> receptor signaling is**  
396 **critical for startle sensitivity.** (A) Bubble plots reporting the level of significance of the top 10  
397 dysregulated proteins for both *cyfip2* heterozygous (top) and mutant (bottom) groups compared to  
398 wildtype controls. The size of the dot is proportional to the significance of the results while the color code  
399 represents the log<sub>2</sub> fold change; top five upregulated (green), and top five downregulated (red) proteins

400 are shown. (B-C) Heat maps displaying the impacted canonical pathways (B) and diseases and biological  
401 functions (C) from IPA functional analysis. The blue-colored gradient indicates the degree of enrichment  
402 for the listed pathways or diseases/functions, as represented by the  $-\log$  of the P value for each  
403 pathway, disease and/or function. (D-E) Sensitivity indices for 5 dpf *cyfip2* sibling (+/) and mutant (-/-)  
404 larvae, treated for 60 minutes prior to testing with muscimol (D) or (E) baclofen. All indices (mean  $\pm$  SD)  
405 were compared using a one-way ANOVA with Sidak's multiple comparisons correction.  $p^* < 0.05$ ,  $p^{**} <$   
406  $0.01$ ;  $p^{***} < 0.001$ ;  $p^{****} < 0.0001$ .

407

## 408 **Discussion**

409 Through its ability to modulate both the actin cytoskeleton and protein translation, Cyfip2  
410 is well-positioned to be a critical factor for many processes in neurodevelopment [33,34,37–  
411 39,45,49]. Further highlighting its importance, Cyfip2 has been implicated in an array of  
412 neuropsychiatric and other conditions, including schizophrenia [62], autism [49,63–65], binge  
413 eating [66–68], obesity [69], amyotrophic lateral sclerosis (ALS) [70,71], Alzheimer's disease  
414 [72], epilepsy [65,73–76], and cancer [77–82]. Here we focused on Cyfip2's role in a common  
415 endophenotype of schizophrenia and autism, increased acoustic startle responsiveness  
416 [4,24,27,28]. By combining conditional transgenesis, CRISPR/Cas9 gene editing,  
417 pharmacology, and discovery proteomics in an *in vivo*, vertebrate model system, we found that  
418 both actin and translational regulation pathways are required for Cyfip2 to establish and  
419 maintain a normal startle threshold. Our data indicate that through these pathways Cyfip2  
420 modulates both excitatory (NMDA receptor) and inhibitory (GABA<sub>B</sub> receptor) function to  
421 establish and maintain proper sensory responsiveness.

422

### 423 Cyfip2 acts through both Rac1 and FMRP to establish the acoustic startle threshold.

424 The actin regulating function of Cyfip2-Rac1 interactions is essential for many  
425 neurodevelopmental processes including neuronal outgrowth and maturation, synapse  
426 formation and function, axon guidance and cell migration [38,44,45,83]. The functional  
427 importance of Cyfip2-FMRP interactions, though less well characterized than Cyfip1-FMRP  
428 interactions, are thought to similarly impact the expression of many key neurodevelopmental

429 proteins that are directly involved in axon growth, synapse maturation, and synaptic plasticity  
430 [34,45,84–86]. Here we used a heatshock-inducible expression system to reveal that Cyfip2  
431 requires the ability to interact with both Rac1 and FMRP to establish the acoustic startle  
432 threshold early in neurodevelopment (Fig. 1E). The ability of wildtype Cyfip2 to restore normal  
433 startle sensitivity in mutant larvae when expression is induced at 30 hpf (Fig. 1D,E), but not at  
434 48, 72, or 96 hpf (Fig. S4) reveals some potential ways that it may affect the underlying neural  
435 circuits. Prior to the rescue window, by 8-15 hpf the command-like Mauthner cells have been  
436 specified [87] and begun extending their axons (17-18 hpf) and lateral dendrites (22-23 hpf)  
437 [88,89]. During the rescue window from ~30-48 hpf, other neurons in the startle circuit continue  
438 to migrate to their final positions in the ventral hindbrain, and the synaptic contacts within the  
439 circuit begin to form and mature, including those between the auditory nerve, Mauthner cells,  
440 and excitatory Spiral Fiber Neurons (SFNs) [89–91]. Actin dynamics would be required during  
441 this time to facilitate neuronal migration, axon and dendrite growth, and synapse formation.  
442 These processes would also require precisely regulated RNA translation through complexes like  
443 Cyfip2-FMRP-eIF4E to produce the many proteins needed to establish these connections.  
444 When we induced Cyfip2 expression at 5 dpf we observed a clear bimodal distribution with  
445 some mutants remaining hypersensitive and a second population with normal sensitivity (Fig.  
446 2A). This pattern was not observed when Rac1 or FMRP binding was abolished, suggesting that  
447 both pathways are also needed for Cyfip2 to modulate the startle circuit in this acute context,  
448 which would likely occur through changes in neuronal and/or synaptic function rather than  
449 altered connectivity. That Cyfip2 expression between 48-96 hpf did not restore the startle  
450 threshold in mutants could be due to insufficient levels, but together our conditional expression  
451 experiments indicate that Cyfip2 is able to most reliably function when the circuit is in a less  
452 mature state.

453 Our findings also show that Cyfip2-Rac1 but not Cyfip2-FMRP binding is required for the  
454 performance of the startle response, as kinematic parameters including latency, turn angle, and

455 duration were largely restored to normal by wildtype and  $\Delta FMRP$  versions of Cyfip2 but  
456 remained altered in  $\Delta Rac1$ -Cyfip2 expressing *cyfip2* mutants (Fig. S1). These data demonstrate  
457 that the actin regulation and translation regulation functions of Cyfip2, while both are required in  
458 some contexts, also have some non-overlapping roles. This is consistent with findings in  
459 zebrafish larvae showing that Cyfip2's interaction with FMRP is dispensable but that its  
460 interaction with the Wave Regulatory Complex (WRC), which like the Rac1-Cyfip2 interaction  
461 regulates actin polymerization (Fig. 1B), is required for retinal ganglion cell (RGC) axons to  
462 properly navigate to their targets in the contralateral optic tectum [45]. In the startle context, our  
463 data showing that  $\Delta FMRP$ -Cyfip2 drives a stronger rescue for turn angle and duration than for  
464 latency suggest that the Cyfip2-FMRP translational regulation pathway contributes more to the  
465 initial sensory processing of acoustic stimuli than the regulation of motor output in the spinal  
466 cord. The actin regulatory function of Cyfip2, however, appears to be critical for all of Cyfip2's  
467 known roles in the startle circuit.

468

#### 469 Cyfip2-dependent startle threshold regulation requires FMRP but not FXR1/2.

470 Previously, we observed that mutants from the *fmr1*<sup>hu2787</sup> line have normal startle  
471 sensitivity, suggesting that FMRP plays no role in regulating the startle threshold [32]. So here  
472 we tested whether Cyfip2, which in contrast to the closely related Cyfip1 has the capacity to also  
473 bind with the Fragile X-related proteins FXR1 and FXR2 [33], may instead rely on these binding  
474 partners to modulate the startle threshold. Like FMRP, both FXR1 and FXR2 regulate RNA  
475 translation [92,93] and are expressed in the brain during early vertebrate neurodevelopment,  
476 though divergent expression patterns emerge for the FXR1/2 proteins in later development and  
477 adulthood in most vertebrates [94–96]. By analyzing FMRP, FXR1, and FXR2 crispants,  
478 however, we found that FXR1 and FXR2 are dispensable but that FMRP is required for normal  
479 startle sensitivity (Fig. 1F). This data is consistent with the distinct expression patterns of the  
480 FMRP, FXR1 and FXR2 proteins, as well as the inability of FXR1/2 to functionally compensate

481 for the loss of FMRP [94–96]. Similarly, in *Drosophila*, which have only one Fragile X protein  
482 family member (dFMR1), re-expressing human FMRP (hFMR1), but not human FXR1 or FXR2,  
483 in dFMR1 mutants is sufficient to specifically rescue aberrant neuronal phenotypes [97]. As  
484 discussed above, the fact that *fmr1* crispants but not *fmr1*<sup>hu2787</sup> mutants show startle  
485 hypersensitivity may be due to genomic adaptation in the ENU-induced *fmr1*<sup>hu2787</sup> line [50]. That  
486 we observed that *fmr1* crispants show heightened startle sensitivity in the *cyfip2* mutant  
487 background compared to *cyfip2* mutants alone (Fig. 1F) further strengthens our conclusion that  
488 Cyfip2 and FMRP work cooperatively to regulate the startle threshold.

489

490 Cyfip2-dependent branched actin dynamics are required for maintaining the acoustic startle  
491 threshold.

492 Our rescue experiments indicate that Cyfip2's actin regulatory function through its  
493 binding with Rac1 is required during startle circuit development (Fig. 1E) and that this pathway  
494 may also facilitate a more acute role for Cyfip2 in maintaining the startle threshold (Fig. 2A).  
495 This conclusion is bolstered by our finding that inhibition of Arp2/3 with 20  $\mu$ M CK-869 for 30  
496 minutes prior to testing uncovers startle hypersensitivity in *cyfip2* heterozygotes but not  
497 wildtypes (Fig. 2B). Thus in wildtypes, Cyfip2 must act acutely to facilitate actin polymerization  
498 to maintain the startle threshold in the face of this challenge. Arp2/3-mediated F-actin nucleation  
499 creates branched actin filaments, while formin-mediated nucleation produces unbranched  
500 filaments [56–58,98]. Our data show that only branched actin nucleation is required for acute  
501 maintenance of the startle threshold, while both formin activity and cofilin-mediated actin  
502 filament severing play no acute role in regulating the startle threshold (Fig. 2C). Formin 2B has  
503 been shown with morpholinos to be required developmentally for normal startle responsiveness,  
504 however, and it appears to play a role in the growth of Spiral Fiber Neuron (SFN) axons [60].  
505 SFNs are excitatory interneurons that receive input from the contralateral auditory nerve and  
506 project their axons across the midline to the contralateral Mauthner cell, providing a key driving

507 force to initiate the startle response [99]. We previously found that SFNs, but not Mauthner cells,  
508 have heightened excitability in *cyfip2* mutants [32], making them a likely place for Cyfip2 to  
509 regulate the startle threshold. Functioning acutely, Cyfip2 may impact synaptic input onto SFNs,  
510 and it is possible that inhibitory and/or excitatory synapses on SFNs may be modulated by  
511 Cyfip2 to maintain the startle threshold. Cyfip1 and Cyfip2 are both enriched at excitatory  
512 synapses and regulate dendritic complexity and spine maturation in mouse cortical neurons  
513 [84,85]. Both Cyfip1 and Cyfip2 are also found at inhibitory postsynaptic sites in mouse  
514 hippocampal neurons, and overexpression of either protein disrupts excitatory/inhibitory (E/I)  
515 synaptic balance [86]. It is likely that Cyfip2 functions similarly in the zebrafish startle circuit to  
516 regulate neuronal excitability, as our data implicate both excitatory (NMDA receptors; Fig. 2D)  
517 and inhibitory (GABA receptors; Fig. 3B,E) pathways.

518

519 Cyfip2 may control sensory processing and other disease-related functions by regulating  
520 neurotransmitter receptors, mitochondrial function, and/or cytoskeletal remodeling.

521 Our candidate drug screen to identify potential downstream effectors of Cyfip2 in  
522 regulating the startle threshold builds on previous work showing that NMDA receptor function is  
523 required for normal startle sensitivity (Fig 2D; Table 1) [61]. While our screen confirmed the  
524 known roles of Cl<sup>-</sup> and K<sup>+</sup> channels, gap junctions, calmodulin, and PDE4 in regulating startle  
525 sensitivity, only the NMDA receptor blocker MK-801 produced a *cyfip2* genotype-specific  
526 response, indicating that Cyfip2 may impact NMDA receptor expression and/or function in the  
527 startle circuit. The mRNAs of three critical NMDA receptor subunit genes – GRIN1, GRIN2A,  
528 and GRIN2B – are all targets of FMRP-mediated translational regulation [100], providing a  
529 potential mechanism for the enhanced sensitivity of *cyfip2* mutants to the NMDAR inhibitor MK-  
530 801. Our unbiased proteomic analysis of *cyfip2* heterozygotes and mutants did not uncover  
531 dysregulation in excitatory synaptic pathways compared to wildtypes, although this may be  
532 because we analyzed protein lysates from whole larvae and thus may have diluted out any

533 changes in NMDA receptor expression in specific neuronal subpopulations. It could also be the  
534 case that *Cyfp2* modulates the membrane localization of NMDA receptors through actin-  
535 mediated trafficking rather than impacting total expression levels.

536         Ingenuity Pathway Analysis (IPA) of our proteomic data revealed that inhibitory GABA  
537 receptor signaling is significantly disrupted in *cyfp2* heterozygotes and mutants (Fig. 3B). We  
538 confirmed that *Cyfp2*-mediated regulation of GABA receptor function plays a key role in the  
539 startle threshold, showing that activation of GABA<sub>B</sub> but not GABA<sub>A</sub> receptors is sufficient to  
540 rescue the startle hypersensitivity phenotype in *cyfp2* mutants (Fig. 3D,E). *Cyfp2* most likely  
541 modulates GABA<sub>B</sub> receptors through translational regulation via FMRP, as both GABA<sub>B</sub> receptor  
542 transcripts in mouse (*GABRAB1* and *GABRAB2*) are targets of FMRP [100]. Further  
543 experiments are needed, though, to determine where and how *Cyfp2* affects GABA<sub>B</sub> receptor  
544 expression in the startle circuit. Our data are consistent with recent findings using rats in which  
545 baclofen-mediated activation of GABA<sub>B</sub> receptors restored normal auditory processing in  
546 *Cntnap2* knockout animals [101]. GABA<sub>B</sub> receptors function both pre-synaptically to regulate  
547 neurotransmitter release and post-synaptically to activate inward-rectifying K<sup>+</sup> channels that  
548 cause hyperpolarization [102,103]. GABA<sub>B</sub> receptors are also expressed at high levels  
549 throughout the auditory system [104], and baclofen treatment has been shown to improve social  
550 avoidance in some individuals with autism [105–107]. It is currently unknown whether baclofen  
551 affects sensory processing in clinical populations, however. Our data fit with a growing body of  
552 evidence that GABA<sub>B</sub> receptors are important modulators of auditory function with direct clinical  
553 applications.

554         The most significantly disrupted pathways in our proteomic analysis of *cyfp2*  
555 heterozygotes and mutants were oxidative phosphorylation and mitochondrial dysfunction (Fig.  
556 3B). It is unclear if these metabolic functions influence the activity of the acoustic startle circuit,  
557 although these pathways are essential within neurons for neuronal development and plasticity,  
558 cell death, axon extension and branching, and synaptogenesis [108,109], and so they may also



559 contribute to the many disease associations for *Cyfip2* listed above. Our data also show that in  
560 the absence of *Cyfip2*, mitochondrial proteins (*ACAD11*, *MT-ND4*) increase in abundance, and  
561 cytoskeletal (*TMSB10/TMSB4X*) and extracellular matrix (ECM) proteins (*COL6A3*, *COL1A1*)  
562 decrease in abundance (Fig 3A; Table S8). *TMSB4X* and *TMSB10* both suppress actin  
563 polymerization [110,111], so their downregulation in *cyfip2* mutants may reflect an attempt to  
564 compensate for the loss of *Cyfip2*- and *WRC*-mediated actin polymerization. ECM collagens like  
565 *COL6A3* and *COL1A1* are important for multiple aspects of neural development including axon  
566 guidance [112,113], and so this may reflect another potential mechanism for *Cyfip2*'s  
567 developmental role in regulating the startle circuit. Our analysis of diseases and functions  
568 impacted by the loss of *Cyfip2* include multiple neurological and neuromuscular conditions (Fig.  
569 3C). These findings reinforce the known associations between *cyfip2* and ALS [70,71] and  
570 Alzheimer's disease [72], further underscoring the importance of *Cyfip2* for neural function  
571 beyond the startle circuit. Further work on the links between *Cyfip2*, its molecular effectors, and  
572 the development, function, and maintenance of neural circuits will improve our understanding of  
573 and ability to treat these varied conditions.

574

## 575 **Materials & Methods**

### 576 Zebrafish Husbandry and Maintenance

577 All animal use and procedures were approved by the North Carolina State University  
578 Institutional Animal Care and Use Committee (IACUC). Zebrafish embryos were obtained from  
579 the Zebrafish International Resource Center (ZIRC), the University of Pennsylvania, or  
580 generated at North Carolina State University and raised in a recirculating housing system.  
581 Animals were fed and housed at a 5 zebrafish/L density under a 14h:10h light-dark cycle at  
582 28°C.

583 Embryos were generated by a male and female pair placed in a mating box  
584 (Aquaneering) containing system water and artificial grass. The following morning, 2-3 hours

585 into the light cycle, embryos were collected in petri dishes containing E3 embryo media (5 mM  
586 NaCl, 0.17 mM KCl, 0.33 mM CaCl<sub>2</sub>·2H<sub>2</sub>O, 0.33 mM MgSO<sub>4</sub> in water). Embryos were  
587 examined under a brightfield compound microscope for fertilization and proper development and  
588 were kept in groups ≤ 65. Embryos were placed in a 29°C incubator on a 14h:10h light-dark  
589 cycle. 50% of E3 media changed daily, and any embryos with gross morphological defects were  
590 removed and euthanized.

#### 591 DNA Extraction & Genotyping

592 Fin biopsies were obtained from adult fish anesthetized in 0.02% Tricaine (MS-222;  
593 Fisher) in system water. Fin clips were taken using a razor blade to remove ~2-3 mm of tissue  
594 from the tail fin and samples were immediately fixed in 100% MeOH. Larval samples were  
595 individually fixed in 100% MeOH following behavioral testing. DNA was extracted using the  
596 HotShot DNA lysis method which consisted of a tissue lysis with base solution (25mM NaOH,  
597 0.2mM EDTA), sample incubation at 95°C for 30 minutes, and sample neutralization with  
598 neutralizing solution (40mM Tris-HCl). *cyfip2*<sup>p400</sup> fish were genotyped using either dCAPS PCR  
599 and restriction digest with Apol-HF [32] or the rhAmp SNP Genotyping System (IDT). rhAmp  
600 SNP genotyping was carried out using *cyfip2* locus and allele specific primers (Table S3)  
601 targeting the wildtype and *cyfip2*<sup>p400</sup> alleles. Genotyping for *Tg(hsp70:cyfip2-GFP)*,  
602 *Tg(hsp70:cyfip2-(C179R)-GFP)* and *Tg(hsp70:cyfip2-(K723E)-GFP)* was accomplished by PCR  
603 amplification with primers specific to GFP (Table S4) followed by agarose gel electrophoresis.

604

#### 605 Molecular Cloning

606 Alternative *cyfip2* rescue constructs ( $\Delta$ *Rac1*;  $\Delta$ *FMRP*) were generated from a pENTR  
607 *cyfip2*-EGFP plasmid [32] using custom primers and the Q5 Site Directed Mutagenesis Kit  
608 (NEB) to induce the desired C179R ( $\Delta$ *Rac1*) and K723E ( $\Delta$ *FMRP*) mutations. Mutagenesis was  
609 confirmed using restriction digest and Sanger sequencing (Table S3). LR Gateway Cloning  
610 (ThermoFisher) was used to insert the altered *cyfip2*-EGFPs into the pDEST I-SceI hsp70

611 destination vector. Transgenic lines were created by microinjection into 1-cell stage embryos  
612 with a transgenesis mix containing phenol red, I-SceI enzyme, and the pDEST I-SceI  
613 hsp70:*cyfip2*-(C179R)-EGFP or pDEST I-SceI hsp70:*cyfip2*-(K723E)-EGFP plasmid.

#### 614 Inducible Heatshock Rescue & Imaging

615 Inducible expression of *cyfip2-EGFP*, as well as C179R and K723E variants, was  
616 initiated at 30 hpf by placing dechorionated larvae into 96-well plates and incubating at 38°C for  
617 15 or 40 minutes [32]. Following heatshock, larvae were returned to Petri dishes, and given 4  
618 days of recovery at 29°C. GFP fluorescence was confirmed between 4-6 hours post-heatshock  
619 for startle experiments using a Nikon SMZ25 stereo microscope with a GFP bandpass filter and  
620 Lumen 200 fluorescence illumination system. For day 5 heatshock rescue experiments, larvae  
621 were given 4 hours of recovery at 29°C prior to startle sensitivity testing.

622 For imaging experiments, larvae were treated as above for transgene expression at 30  
623 hpf and at 29°C for 1 hour recovered in petri dishes in groups  $\leq 65$ . After 1 hour of recovery  
624 fluorescence was verified, and larvae were visualized using the stereo microscope system  
625 described above and larval images were captured at 1-, 3-, 6-, 18-, 24-, 30-, and 42-hours post-  
626 heatshock using a Nikon DS-Qi2 monochrome microscope camera. Image analysis was  
627 conducted using FIJI (ImageJ) analysis software to manually define ROIs encompassing the  
628 entire larval body, excluding the eye and auto fluorescent yolk sac. Fluorescence intensity  
629 values reflect the mean gray values recorded for respective ROIs.

#### 630 Chemical Exposures

631 For all exposures, groups of 10-20 larvae (5 dpf) were incubated for specified periods of  
632 between 30 minutes and 16 hours within 35 mm Petri dishes in 2 mL of each drug solution.  
633 Drug solutions remained on larvae during startle testing for 30 minutes to 1-hour exposures. For  
634 16-hour incubations larvae first received fresh E3 prior to testing. Following incubation, larvae  
635 were placed on the 6x6 acrylic testing grid and run through the acoustic startle assay. CK-869,  
636 CK-666, MK-801, *N*-phenylanthranilic acid (NPAA), meclofenamic acid (MA),

637 phenoxybenzamine (POBA), etazolate (ETAZ), BMS 204352, muscimol, and baclofen were  
638 obtained from Sigma-Aldrich. SMIFH2, IPA-3, GSK429286 and NSC23766 were acquired from  
639 Tocris through Fisher Scientific.

#### 640 Behavioral Assays

641 All larvae were tested at 5 days post-fertilization (dpf) unless otherwise stated. On the  
642 day of testing, embryos were thoroughly screened for developmental defects, and those with  
643 gross morphological defects were removed prior to behavior testing. *cyfip2*<sup>p400</sup> larvae without  
644 inflated swim bladders were not discarded, as *cyfip2* mutant larvae fail to inflate their swim  
645 bladders [32]. Larvae were adapted to the testing arena lighting and temperature conditions for  
646 30 minutes prior to testing. As previously described, the behavioral testing system consists of a  
647 36-well acrylic grid attached to an acoustic-vibrational shaker (Bruel-Kjaer), a photron mini UX-  
648 50 camera, LED lighting, InfraRed illuminator, and an acrylic IR diffuser [5,32,61].

649 To test the acoustic startle response, 5 dpf larvae were presented with 60 total stimuli  
650 with a 20 second interstimulus interval (ISI), with 10 pseudo-randomized trials at each of the  
651 following 6 stimulus intensities: 13.6, 25.7, 29.2, 35.5, 39.6 and 53.6 dB. All stimuli were  
652 calibrated using a PCB Piezotronics accelerometer (#355B04) and signal conditioner  
653 (#482A21), and voltage outputs were converted to dB using the formula  $\text{dB} = 20 \log (V/0.775)$   
654 [32].

#### 655 Behavioral Analysis

656 All responses in the acoustic startle assay were tracked using FLOTE analysis software  
657 [5,32,61]. Short latency C-bends (SLCs) were identified by FLOTE using defined kinematic  
658 parameters (latency, turn angle, duration, and maximum angular velocity). Startle sensitivity was  
659 calculated by measuring the SLC frequency at each of the six stimulus intensities during the 60-  
660 stimulus startle assay. Sensitivity indices were defined as the area under the startle frequency  
661 vs. stimulus intensity curve calculated using Prism software (GraphPad).

#### 662 Larval Sample Preparation for Proteomics.

663 Larvae from incrosses of *cyfip2*<sup>+/*p400*</sup> carriers were raised as described above. At 3 dpf, DNA was  
664 extracted from larvae using the Zebrafish Embryonic Genotyping (ZEG) apparatus (DanioLab).  
665 ZEG samples were used for PCR amplification and then submitted for Sanger sequencing to  
666 determine the genotype at the *cyfip2*<sup>*p400*</sup> locus. At 5 dpf larvae were sorted into pools of 30  
667 larvae for each genotype: homozygous wild type, *cyfip2*<sup>*p400*</sup> heterozygous, and homozygous  
668 mutant. Samples were snap frozen in liquid nitrogen and stored at -80°C. They were then  
669 resuspended and lysed in 100 µL ammonium bicarbonate (ABC; pH 8) containing 1% sodium  
670 deoxycholate (SDC) using a Branson SLPe Sonicator (40:0.15;4C) delivering two 20 second  
671 pulses at 20% amplitude intensity separated by 10 seconds between pulses. Lysates were  
672 centrifuged at 10,000 rpm for 5 minutes at 4°C, and the supernatants were retained and  
673 quantified using Pierce BCA protein quantification (ThermoFisher; Cat #: 23225) and an  
674 IMPLEN NP80 nanophotometer. Lysates were submitted the same-day to the Molecular  
675 Education, Technology and Research Innovation Center (METRIC) at NC State University for  
676 protein digestion and LC-MS.

#### 677 Protein Digestion and LC-MS

678 Each lysed sample was normalized to 200 µg of protein in 200 µL of ABC/SDC solution.  
679 Disulfide reduction was conducted by adding 15 µL 50 mM DTT and incubating at 56°C for 30  
680 minutes. 200 µL of 8M urea in 0.1 M Tris buffer (pH 8) was added and samples were transferred  
681 to Vivicon 30kD Molecular Weight Cut-off (MWCO) filters. Samples were centrifuged at 12,000 x  
682 g for 10 minutes at 21°C. 200 µL of 8 M urea in 0.1 M Tris buffer (pH 8) was added to the top of  
683 each filter, as well as 64 µL 55 mM iodoacetamide (IAA) solution and samples were incubated  
684 for 1 hour in the dark at room temperature. Samples were centrifuged at 12,000 x g for 20  
685 minutes. 100 µL of 2 M urea, 10 mM CaCl<sub>2</sub> in 0.1 M Tris buffer (pH 8) was added and samples  
686 were centrifuged at 12,000 x g for 20 minutes. The previous step was repeated twice. 100 µL of  
687 0.1 M Tris buffer (pH 7.5) was added and samples were centrifuged at 12,000 x g for 20-45  
688 minutes. This step was repeated twice, with a 1-hour centrifuge period on the final spin. 200 µL

689 of 0.02 µg/mL trypsin in 0.1 M Tris buffer (pH 7.5) was added, and samples incubated overnight  
690 at 37°C. Following protein digestion with trypsin, samples were placed into fresh microcentrifuge  
691 reservoirs, and 50 µL of quench solution (0.001% zwittergent3-16 in water, 1% formic acid) was  
692 added and samples centrifuged at 12,000 x g for 1 hour. 450 µL quench solution was applied to  
693 each filter and samples were centrifuged at 14,000 x g for 1 hour. Solutions were dried using a  
694 speedvac concentrator and samples were stored dry until LC-MS. Samples were reconstituted  
695 in 100 µL of mobile phase A (98% water, 2% acetonitrile, 0.1% formic acid) and peptides were  
696 quantified via Pierce BCA assay. Samples were normalized to the lowest peptide concentration  
697 for every sample and nanoLC-MS was conducted using a Thermo Orbitrap Exploris 480. This  
698 work was performed in part by METRIC at NC State University, which is supported by the State  
699 of North Carolina.

#### 700 Proteomics data analysis

701 Shotgun proteomics raw files were processed and quantified with MaxQuant (version 2.2.0.0).  
702 Briefly, the built-in Andromeda search engine scored MS2 spectra against fragment masses of  
703 tryptic peptides derived from a *Danio rerio* reference proteome containing 93,351 entries  
704 including isoforms (UniProt, accessed March 22, 2019). Our database search required variable  
705 modifications (methionine oxidation and N-terminal acetylation) and a fixed modification  
706 (cysteine carbamido-methylation) along with a minimum peptide length of 7 amino acids and  
707 limited the search space to a maximum peptide mass of 4600 Da and a maximum of two missed  
708 cleavages. The false discovery rate was controlled with a target-decoy approach at less than  
709 1% for peptide spectrum matches and protein group identifications.

#### 710 Bioinformatics

711 Label-Free quantification (LFQ) intensities from MaxQuant were imported into Perseus software  
712 (version 2.0.7.0) and transformed to logarithmic scale with base two. Missing values were

713 replaced with values from the normal distribution, reducing the distributions to a factor of “0.3”  
714 (width) and down-shifting by “1.8” standard deviations while simulating random values to  
715 replace the missing values. This protein quantification was used to measure the fold-enrichment  
716 between *cyfip2*<sup>p400</sup> heterozygous/homozygous and *cyfip2* wildtype groups. Statistical  
717 significance was calculated using a two-way Student t-test and FPR (p<0.05). Differentially  
718 expressed proteins (DEPs) were submitted to ingenuity pathway analysis (IPA) to identify their  
719 function, specific processes, and related enriched pathways/diseases.

## 720 Statistical Methods

721 All statistical analyses were performed using Prism (GraphPad). All data sets were tested for  
722 normality in Prism. Subsequent parametric or non-parametric tests and post-hoc analyses were  
723 performed using Prism, and significance values (p < 0.05) were reported.

724

## 725 Acknowledgements

726 We would like to thank Leonard Collins and Taufika Williams from METRIC at NC State  
727 University for their assistance with proteomic analysis. A special thank you to Kimberly Scofield  
728 and Kara Carlson for feedback on the manuscript.

729

## 730 Funding Disclosure

731 We are grateful for financial support from the National Institute for Neurological Disease and  
732 Stroke (R01-NS116354 to K.C.M.) and for seed funds provided by North Carolina State  
733 University’s Center for Human Health and the Environment (CHHE) through a National Institute  
734 of Environmental Health Science center grant (P30 ES025128).

735

736 **Competing Interests**

737 The authors declare that no competing interests exist.

738

739 **References**

- 740 1. Burgess HA, Granato M. Modulation of locomotor activity in larval zebrafish during light  
741 adaptation. *J Exp Biol.* 2007;210: 2526–2539. doi:10.1242/jeb.003939
- 742 2. Vagnoni E, Lourenco SF, Longo MR. Threat modulates perception of looming visual  
743 stimuli. *Curr Biol.* 2012;22: R826-7. doi:10.1016/j.cub.2012.07.053
- 744 3. Randlett O, Haesemeyer M, Forkin G, Shoenhard H, Schier AF, Engert F, et al. Distributed  
745 Plasticity Drives Visual Habituation Learning in Larval Zebrafish. *Curr Biol.* 2019;29: 1337-  
746 1345.e4. doi:10.1016/j.cub.2019.02.039
- 747 4. Geyer MA, Swerdlow NR, Mansbach RS, Braff DL. Startle response models of  
748 sensorimotor gating and habituation deficits in schizophrenia. *Brain Res Bull.* 1990;25:  
749 485–498. doi:10.1016/0361-9230(90)90241-q
- 750 5. Burgess HA, Granato M. Sensorimotor gating in larval zebrafish. *J Neurosci.* 2007;27:  
751 4984–4994. doi:27/18/4984 [pii]
- 752 6. Weidenmüller A, Kleineidam C, Tautz J. Collective control of nest climate parameters in  
753 bumblebee colonies. *Anim Behav.* 2002;63: 1065–1071. doi:10.1006/anbe.2002.3020
- 754 7. Weidenmuller A. The control of nest climate in bumblebee (*Bombus terrestris*) colonies:  
755 interindividual variability and self reinforcement in fanning response. *Behav Ecol.* 2004;15:  
756 120–128. doi:10.1093/beheco/arg101
- 757 8. Ward AJW, Sumpter DJT, Couzin ID, Hart PJB, Krause J. Quorum decision-making  
758 facilitates information transfer in fish shoals. *Proc Natl Acad Sci U S A.* 2008;105: 6948–  
759 6953. doi:10.1073/pnas.0710344105
- 760 9. Cresci A, De Rosa R, Agnisola C. Assessing the Influence of Personality on Sensitivity to  
761 Magnetic Fields in Zebrafish. *J Vis Exp.* 2019. doi:10.3791/59229
- 762 10. Michel WC, Sanderson MJ, Olson JK, Lipschitz DL. Evidence of a novel transduction  
763 pathway mediating detection of polyamines by the zebrafish olfactory system. *J Exp Biol.*  
764 2003;206: 1697–1706. doi:10.1242/jeb.00339
- 765 11. Dudova I, Vodicka J, Havlovicova M, Sedlacek Z, Urbanek T, Hrdlicka M. Odor detection  
766 threshold, but not odor identification, is impaired in children with autism. *Eur Child Adolesc*  
767 *Psychiatry.* 2011;20: 333–340. doi:10.1007/s00787-011-0177-1
- 768 12. Tavassoli T, Baron-Cohen S. Olfactory detection thresholds and adaptation in adults with  
769 autism spectrum condition. *J Autism Dev Disord.* 2012;42: 905–909. doi:10.1007/s10803-  
770 011-1321-y



- 771 13. Takahashi H, Tsuboi A. Olfactory avoidance test (mouse). *Bio Protoc.* 2017;7: e2153.  
772 doi:10.21769/BioProtoc.2153
- 773 14. Blakemore S-J, Tavassoli T, Calò S, Thomas RM, Catmur C, Frith U, et al. Tactile  
774 sensitivity in Asperger syndrome. *Brain Cogn.* 2006;61: 5–13.  
775 doi:10.1016/j.bandc.2005.12.013
- 776 15. Kohashi T, Oda Y. Initiation of Mauthner- or non-Mauthner-mediated fast escape evoked  
777 by different modes of sensory input. *J Neurosci.* 2008;28: 10641–10653.  
778 doi:10.1523/JNEUROSCI.1435-08.2008
- 779 16. DeLorey TM, Sahbaie P, Hashemi E, Li W-W, Salehi A, Clark DJ. Somatosensory and  
780 sensorimotor consequences associated with the heterozygous disruption of the autism  
781 candidate gene, *Gabrb3*. *Behav Brain Res.* 2011;216: 36–45.  
782 doi:10.1016/j.bbr.2010.06.032
- 783 17. Puts NAJ, Wodka EL, Tommerdahl M, Mostofsky SH, Edden RAE. Impaired tactile  
784 processing in children with autism spectrum disorder. *J Neurophysiol.* 2014;111: 1803–  
785 1811. doi:10.1152/jn.00890.2013
- 786 18. Armington JC. The electroretinogram, the visual evoked potential, and the area-luminance  
787 relation. *Vision Res.* 1968;8: 263–276. doi:10.1016/0042-6989(68)90014-x
- 788 19. Campbell FW, Maffei L. The influence of spatial frequency and contrast on the perception  
789 of moving patterns. *Vision Res.* 1981;21: 713–721. doi:10.1016/0042-6989(81)90080-8
- 790 20. Yilmaz M, Meister M. Rapid innate defensive responses of mice to looming visual stimuli.  
791 *Curr Biol.* 2013;23: 2011–2015. doi:10.1016/j.cub.2013.08.015
- 792 21. Wang Y, Wu W, Zhang X, Hu X, Li Y, Lou S, et al. A Mouse Model of Visual Perceptual  
793 Learning Reveals Alterations in Neuronal Coding and Dendritic Spine Density in the Visual  
794 Cortex. *Front Behav Neurosci.* 2016;10: 42. doi:10.3389/fnbeh.2016.00042
- 795 22. Bakker MJ, Tijssen MA, van der Meer JN, Koelman JH, Boer F. Increased whole-body  
796 auditory startle reflex and autonomic reactivity in children with anxiety disorders. *J*  
797 *Psychiatry Neurosci.* 2009;34: 314–322. Available:  
798 <https://www.ncbi.nlm.nih.gov/pubmed/19568483>
- 799 23. Han K, Chen H, Gennarino VA, Richman R, Lu H-C, Zoghbi HY. Fragile X-like behaviors  
800 and abnormal cortical dendritic spines in cytoplasmic FMR1-interacting protein 2-mutant  
801 mice. *Hum Mol Genet.* 2015;24: 1813–1823. doi:10.1093/hmg/ddu595
- 802 24. Takahashi H, Nakahachi T, Stickley A, Ishitobi M, Kamio Y. Relationship between  
803 physiological and parent-observed auditory over-responsiveness in children with typical  
804 development and those with autism spectrum disorders. *Autism.* 2018;22: 291–298.  
805 doi:10.1177/1362361316680497 [doi]
- 806 25. Grillon C, Ameli R, Goddard A, Woods SW, Davis M. Baseline and fear-potentiated startle  
807 in panic disorder patients. *Biol Psychiatry.* 1994;35: 431–439. doi:10.1016/0006-  
808 3223(94)90040-x

- 809 26. Grillon C, Davis M. Acoustic startle and anticipatory anxiety in humans: effects of monaural  
810 right and left ear stimulation. *Psychophysiology*. 1995;32: 155–161. doi:10.1111/j.1469-  
811 8986.1995.tb03307.x [doi]
- 812 27. Chamberlain PD, Rodgers J, Crowley MJ, White SE, Freston MH, South M. A potentiated  
813 startle study of uncertainty and contextual anxiety in adolescents diagnosed with autism  
814 spectrum disorder. *Mol Autism*. 2013;4: 31. doi:10.1186/2040-2392-4-31
- 815 28. Kohl S, Heekeren K, Klosterkötter J, Kuhn J. Prepulse inhibition in psychiatric disorders--  
816 apart from schizophrenia. *J Psychiatr Res*. 2013;47: 445–452.  
817 doi:10.1016/j.jpsychires.2012.11.018
- 818 29. Eaton RC, Bombardieri RA, Meyer DL. The Mauthner-initiated startle response in teleost  
819 fish. *J Exp Biol*. 1977;66: 65–81. doi:10.1242/jeb.66.1.65
- 820 30. Kimmel CB, Patterson J, Kimmel RO. The development and behavioral characteristics of  
821 the startle response in the zebra fish. *Dev Psychobiol*. 1974;7: 47–60.  
822 doi:10.1002/dev.420070109
- 823 31. Davis M, Gendelman DS, Tischler MD, Gendelman PM. A primary acoustic startle circuit:  
824 lesion and stimulation studies. *J Neurosci*. 1982;2: 791–805. doi:10.1523/JNEUROSCI.02-  
825 06-00791.1982
- 826 32. Marsden KC, Jain RA, Wolman MA, Echeverry FA, Nelson JC, Hayer KE, et al. A Cyfip2-  
827 Dependent Excitatory Interneuron Pathway Establishes the Innate Startle Threshold. *Cell*  
828 *Rep*. 2018;23: 878–887. doi:S2211-1247(18)30471-6 [pii]
- 829 33. Schenck A, Bardoni B, Moro A, Bagni C, Mandel JL. A highly conserved protein family  
830 interacting with the fragile X mental retardation protein (FMRP) and displaying selective  
831 interactions with FMRP-related proteins FXR1P and FXR2P. *Proc Natl Acad Sci U S A*.  
832 2001;98: 8844–8849. doi:10.1073/pnas.151231598 [doi]
- 833 34. Napoli I, Mercaldo V, Boyl PP, Eleuteri B, Zalfa F, Rubeis SD, et al. The fragile X syndrome  
834 protein represses activity-dependent translation through CYFIP1, a new 4E-BP. *Cell*.  
835 2008;134: 1042–1054. doi:10.1016/j.cell.2008.07.031 [doi]
- 836 35. Kobayashi K, Kuroda S, Fukata M, Nakamura T, Nagase T, Nomura N, et al. p140Sra-1  
837 (specifically Rac1-associated protein) is a novel specific target for Rac1 small GTPase. *J*  
838 *Biol Chem*. 1998;273: 291–295. doi:10.1074/jbc.273.1.291 [doi]
- 839 36. Eden S, Rohatgi R, Podtelejnikov AV, Mann M, Kirschner MW. Mechanism of regulation of  
840 WAVE1-induced actin nucleation by Rac1 and Nck. *Nature*. 2002;418: 790–793.  
841 doi:10.1038/nature00859
- 842 37. Schenck A, Bardoni B, Langmann C, Harden N, Mandel JL, Giangrande A. CYFIP/Sra-1  
843 controls neuronal connectivity in *Drosophila* and links the Rac1 GTPase pathway to the  
844 fragile X protein. *Neuron*. 2003;38: 887–898. doi:S0896627303003544 [pii]
- 845 38. Bogdan S, Grewe O, Strunk M, Mertens A, Klämbt C. Sra-1 interacts with Kette and Wasp  
846 and is required for neuronal and bristle development in *Drosophila*. *Development*.  
847 2004;131: 3981–3989. doi:10.1242/dev.01274

- 848 39. Chen Z, Borek D, Padrick SB, Gomez TS, Metlagel Z, Ismail AM, et al. Structure and  
849 control of the actin regulatory WAVE complex. *Nature*. 2010;468: 533–538.  
850 doi:10.1038/nature09623 [doi]
- 851 40. Chen B, Padrick SB, Henry L, Rosen MK. Biochemical reconstitution of the WAVE  
852 regulatory complex. *Methods Enzymol*. 2014;540: 55–72. doi:10.1016/B978-0-12-397924-  
853 7.00004-2
- 854 41. Chen B, Chou HT, Brautigam CA, Xing W, Yang S, Henry L, et al. Rac1 GTPase activates  
855 the WAVE regulatory complex through two distinct binding sites. *Elife*. 2017;6:  
856 10.7554/eLife.29795. doi:10.7554/eLife.29795 [doi]
- 857 42. Trowe T, Klostermann S, Baier H, Granato M, Crawford AD, Grunewald B, et al. Mutations  
858 disrupting the ordering and topographic mapping of axons in the retinotectal projection of  
859 the zebrafish, *Danio rerio*. *Development*. 1996;123: 439–450. doi:10.1242/dev.123.1.439
- 860 43. Schenck A, Qurashi A, Carrera P, Bardoni B, Diebold C, Schejter E, et al. WAVE/SCAR, a  
861 multifunctional complex coordinating different aspects of neuronal connectivity. *Dev Biol*.  
862 2004;274: 260–270. doi:10.1016/j.ydbio.2004.07.009
- 863 44. Pittman AJ, Gaynes JA, Chien CB. Nev (Cyfip2) is Required for Retinal Lamination and  
864 Axon Guidance in the Zebrafish Retinotectal System. *Dev Biol*. 2010;344: 784–794.  
865 doi:10.1016/j.ydbio.2010.05.512 [doi]
- 866 45. Cioni JM, Wong HH, Bressan D, Kodama L, Harris WA, Holt CE. Axon-Axon Interactions  
867 Regulate Topographic Optic Tract Sorting via CYFIP2-Dependent WAVE Complex  
868 Function. *Neuron*. 2018;97: 1078-1093.e6. doi:S0896-6273(18)30052-7 [pii]
- 869 46. Lee Y, Kim D, Ryu JR, Zhang Y, Kim S, Kim Y, et al. Phosphorylation of CYFIP2, a  
870 component of the WAVE-regulatory complex, regulates dendritic spine density and neurite  
871 outgrowth in cultured hippocampal neurons potentially by affecting the complex assembly.  
872 *Neuroreport*. 2017;28: 749–754. doi:10.1097/WNR.0000000000000838
- 873 47. Zhang Y, Kang Hyae R, Lee S-H, Kim Y, Ma R, Jin C, et al. Enhanced Prefrontal Neuronal  
874 Activity and Social Dominance Behavior in Postnatal Forebrain Excitatory Neuron-Specific  
875 Cyfip2 Knock-Out Mice. *Front Mol Neurosci*. 2020;13: 574947.  
876 doi:10.3389/fnmol.2020.574947
- 877 48. Kumar V, Kim K, Joseph C, Kourrich S, Yoo SH, Huang HC, et al. C57BL/6N mutation in  
878 cytoplasmic FMRP interacting protein 2 regulates cocaine response. *Science*. 2013;342:  
879 1508–1512. doi:10.1126/science.1245503 [doi]
- 880 49. Abekhouk S, Bardoni B. CYFIP family proteins between autism and intellectual disability:  
881 links with Fragile X syndrome. *Front Cell Neurosci*. 2014;8: 81.  
882 doi:10.3389/fncel.2014.00081 [doi]
- 883 50. Barthelson K, Baer L, Dong Y, Hand M, Pujic Z, Newman M, et al. Zebrafish chromosome  
884 14 gene differential expression in the *fmr1* h u2787 model of Fragile X syndrome. *Front*  
885 *Genet*. 2021;12: 625466. doi:10.3389/fgene.2021.625466

- 886 51. Hu J, Chen L, Yin J, Yin H, Huang Y, Tian J. Hyperactivity, memory defects, and  
887 craniofacial abnormalities in zebrafish *fmr1* mutant larvae. *Behav Genet.* 2020;50: 152–  
888 160. doi:10.1007/s10519-020-09995-7
- 889 52. Zhu SI, McCullough MH, Pujic Z, Sibberas J, Sun B, Darveniza T, et al. *fmr1* Mutation  
890 Alters the Early Development of Sensory Coding and Hunting and Social Behaviors in  
891 Larval Zebrafish. *J Neurosci.* 2023;43: 1211–1224. doi:10.1523/JNEUROSCI.1721-  
892 22.2022
- 893 53. Constantin L, Poulsen RE, Scholz LA, Favre-Bulle IA, Taylor MA, Sun B, et al. Altered  
894 brain-wide auditory networks in a zebrafish model of fragile X syndrome. *BMC Biol.*  
895 2020;18: 125. doi:10.1186/s12915-020-00857-6
- 896 54. Spence EF, Soderling SH. Actin Out: Regulation of the Synaptic Cytoskeleton. *J Biol*  
897 *Chem.* 2015;290: 28613–28622. doi:10.1074/jbc.R115.655118 [doi]
- 898 55. Chalkia D, Nikolaidis N, Makalowski W, Klein J, Nei M. Origins and evolution of the formin  
899 multigene family that is involved in the formation of actin filaments. *Mol Biol Evol.* 2008;25:  
900 2717–2733. doi:10.1093/molbev/msn215
- 901 56. Pellegrin S, Mellor H. The Rho family GTPase Rif induces filopodia through mDia2. *Curr*  
902 *Biol.* 2005;15: 129–133. doi:10.1016/j.cub.2005.01.011
- 903 57. Schirenbeck A, Bretschneider T, Arasada R, Schleicher M, Faix J. The Diaphanous-related  
904 formin dDia2 is required for the formation and maintenance of filopodia. *Nat Cell Biol.*  
905 2005;7: 619–625. doi:10.1038/ncb1266
- 906 58. Peng J, Wallar BJ, Flanders A, Swiatek PJ, Alberts AS. Disruption of the Diaphanous-  
907 related formin *Drf1* gene encoding mDia1 reveals a role for *Drf3* as an effector for *Cdc42*.  
908 *Curr Biol.* 2003;13: 534–545. doi:10.1016/s0960-9822(03)00170-2
- 909 59. Maciver SK, Hussey PJ. The ADF/cofilin family: actin-remodeling proteins. *Genome Biol.*  
910 2002;3: reviews3007. doi:10.1186/gb-2002-3-5-reviews3007
- 911 60. Nagar D, James TK, Mishra R, Guha S, Burgess SM, Ghose A. The Formin *Fmn2b* Is  
912 Required for the Development of an Excitatory Interneuron Module in the Zebrafish  
913 Acoustic Startle Circuit. *eNeuro.* 2021;8. doi:10.1523/ENEURO.0329-20.2021
- 914 61. Wolman MA, Jain RA, Liss L, Granato M. Chemical modulation of memory formation in  
915 larval zebrafish. *Proc Natl Acad Sci U S A.* 2011;108: 15468–15473.  
916 doi:10.1073/pnas.1107156108 [doi]
- 917 62. Focking M, Lopez LM, English JA, Dicker P, Wolff A, Brindley E, et al. Proteomic and  
918 genomic evidence implicates the postsynaptic density in schizophrenia. *Mol Psychiatry.*  
919 2015;20: 424–432. doi:10.1038/mp.2014.63 [doi]
- 920 63. Hoeffler CA, Sanchez E, Hagerman RJ, Mu Y, Nguyen DV, Wong H, et al. Altered mTOR  
921 signaling and enhanced CYFIP2 expression levels in subjects with fragile X syndrome.  
922 *Genes Brain Behav.* 2012;11: 332–341. doi:10.1111/j.1601-183X.2012.00768.x [doi]

- 923 64. Noroozi R, Omrani MD, Sayad A, Taheri M, Ghafouri-Fard S. Cytoplasmic FMRP  
924 interacting protein 1/2 (CYFIP1/2) expression analysis in autism. *Metab Brain Dis.* 2018;33:  
925 1353–1358. doi:10.1007/s11011-018-0249-8 [doi]
- 926 65. Zweier M, Begemann A, McWalter K, Cho MT, Abela L, Banka S, et al. Spatially clustering  
927 de novo variants in CYFIP2, encoding the cytoplasmic FMRP interacting protein 2, cause  
928 intellectual disability and seizures. *Eur J Hum Genet.* 2019;27: 747–759.  
929 doi:10.1038/s41431-018-0331-z
- 930 66. Kirkpatrick SL, Goldberg LR, Yazdani N, Babbs RK, Wu J, Reed ER, et al. Cytoplasmic  
931 FMR1-Interacting Protein 2 Is a Major Genetic Factor Underlying Binge Eating. *Biol*  
932 *Psychiatry.* 2017;81: 757–769. doi:10.1016/j.biopsych.2016.10.021
- 933 67. Babbs RK, Beierle JA, Ruan QT, Kelliher JC, Chen MM, Feng AX, et al. Cyfip1  
934 Haploinsufficiency Increases Compulsive-Like Behavior and Modulates Palatable Food  
935 Intake in Mice: Dependence on Cyfip2 Genetic Background, Parent-of Origin, and Sex. *G3*  
936 . 2019;9: 3009–3022. doi:10.1534/g3.119.400470
- 937 68. Babbs RK, Beierle JA, Yao EJ, Kelliher JC, Medeiros AR, Anandakumar J, et al. The effect  
938 of the demyelinating agent cuprizone on binge-like eating of sweetened palatable food in  
939 female and male C57BL/6 substrains. *Appetite.* 2020;150: 104678.  
940 doi:10.1016/j.appet.2020.104678
- 941 69. Manigandan S, Yun JW. Loss of cytoplasmic FMR1-interacting protein 2 (CYFIP2) induces  
942 browning in 3T3-L1 adipocytes via repression of GABA-BR and activation of mTORC1. *J*  
943 *Cell Biochem.* 2022;123: 863–877. doi:10.1002/jcb.30231
- 944 70. Nachmany H, Wald S, Abekasis M, Bulvik S, Weil M. Two potential biomarkers identified in  
945 mesenchymal stem cells and leukocytes of patients with sporadic amyotrophic lateral  
946 sclerosis. *Dis Markers.* 2012;32: 211–220. doi:10.3233/DMA-2011-0885
- 947 71. Lilo E, Wald-Altman S, Solmesky LJ, Ben Yaakov K, Gershoni-Emek N, Bulvik S, et al.  
948 Characterization of human sporadic ALS biomarkers in the familial ALS transgenic  
949 mSOD1(G93A) mouse model. *Hum Mol Genet.* 2013;22: 4720–4725.  
950 doi:10.1093/hmg/ddt325
- 951 72. Tiwari SS, Mizuno K, Ghosh A, Aziz W, Troakes C, Daoud J, et al. Alzheimer-related  
952 decrease in CYFIP2 links amyloid production to tau hyperphosphorylation and memory  
953 loss. *Brain.* 2016;139: 2751–2765. doi:10.1093/brain/aww205
- 954 73. Nakashima M, Kato M, Aoto K, Shiina M, Belal H, Mukaida S, et al. De novo hotspot  
955 variants in CYFIP2 cause early-onset epileptic encephalopathy. *Ann Neurol.* 2018;83: 794–  
956 806. doi:10.1002/ana.25208 [doi]
- 957 74. Begemann A, Sticht H, Begtrup A, Vitobello A, Faivre L, Banka S, et al. New insights into  
958 the clinical and molecular spectrum of the novel CYFIP2-related neurodevelopmental  
959 disorder and impairment of the WRC-mediated actin dynamics. *Genet Med.* 2021;23: 543–  
960 554. doi:10.1038/s41436-020-01011-x

- 961 75. Biembengut ÍV, Silva ILZ, Souza T de ACB de, Shigunov P. Cytoplasmic FMR1 interacting  
962 protein (CYFIP) family members and their function in neural development and disorders.  
963 Mol Biol Rep. 2021;48: 6131–6143. doi:10.1007/s11033-021-06585-6
- 964 76. Biembengut ÍV, Shigunov P, Frota NF, Lourenzoni MR, de Souza TACB. Molecular  
965 Dynamics of CYFIP2 Protein and Its R87C Variant Related to Early Infantile Epileptic  
966 Encephalopathy. Int J Mol Sci. 2022;23. doi:10.3390/ijms23158708
- 967 77. Takahashi H, Nemoto T, Yoshida T, Honda H, Hasegawa T. Cancer diagnosis marker  
968 extraction for soft tissue sarcomas based on gene expression profiling data by using  
969 projective adaptive resonance theory (PART) filtering method. BMC Bioinformatics. 2006;7:  
970 399. doi:10.1186/1471-2105-7-399
- 971 78. Mongroo PS, Noubissi FK, Cuatrecasas M, Kalabis J, King CE, Johnstone CN, et al. IMP-1  
972 displays cross-talk with K-Ras and modulates colon cancer cell survival through the novel  
973 proapoptotic protein CYFIP2. Cancer Res. 2011;71: 2172–2182. doi:10.1158/0008-  
974 5472.CAN-10-3295
- 975 79. Jiao S, Li N, Cai S, Guo H, Wen Y. Inhibition of CYFIP2 promotes gastric cancer cell  
976 proliferation and chemoresistance to 5-fluorouracil through activation of the Akt signaling  
977 pathway. Oncol Lett. 2017;13: 2133–2140. doi:10.3892/ol.2017.5743
- 978 80. Vandamme T, Beyens M, Boons G, Schepers A, Kamp K, Biermann K, et al. Hotspot  
979 DAXX, PTCH2 and CYFIP2 mutations in pancreatic neuroendocrine neoplasms. Endocr  
980 Relat Cancer. 2019;26: 1–12. doi:10.1530/ERC-18-0120
- 981 81. Liu Y, Liu H, Bian Q. Identification of Potential Biomarkers Associated with Basal Cell  
982 Carcinoma. Biomed Res Int. 2020;2020: 2073690. doi:10.1155/2020/2073690
- 983 82. Li Y, Song X, Liu L, Yue L. NUA2 silencing inhibits the proliferation, migration and  
984 epithelial-to-mesenchymal transition of cervical cancer cells via upregulating CYFIP2. Mol  
985 Med Rep. 2021;24. doi:10.3892/mmr.2021.12457
- 986 83. Steffen A, Rottner K, Ehinger J, Innocenti M, Scita G, Wehland J, et al. Sra-1 and Nap1 link  
987 Rac to actin assembly driving lamellipodia formation. EMBO J. 2004;23: 749–759.  
988 doi:10.1038/sj.emboj.7600084
- 989 84. Rubeis SD, Pasciuto E, Li KW, Fernandez E, Marino DD, Buzzi A, et al. CYFIP1  
990 coordinates mRNA translation and cytoskeleton remodeling to ensure proper dendritic  
991 spine formation. Neuron. 2013;79: 1169–1182. doi:10.1016/j.neuron.2013.06.039 [doi]
- 992 85. Pathania M, Davenport EC, Muir J, Sheehan DF, Lopez-Domenech G, Kittler JT. The  
993 autism and schizophrenia associated gene CYFIP1 is critical for the maintenance of  
994 dendritic complexity and the stabilization of mature spines. Transl Psychiatry. 2014;4:  
995 e374. doi:10.1038/tp.2014.16 [doi]
- 996 86. Davenport EC, Szulc BR, Drew J, Taylor J, Morgan T, Higgs NF, et al. Autism and  
997 Schizophrenia-Associated CYFIP1 Regulates the Balance of Synaptic Excitation and  
998 Inhibition. Cell Rep. 2019;26: 2037-2051.e6. doi:S2211-1247(19)30129-9 [pii]

- 999 87. Hanneman E, Trevarrow B, Metcalfe WK, Kimmel CB, Westerfield M. Segmental pattern of  
1000 development of the hindbrain and spinal cord of the zebrafish embryo. *Development*.  
1001 1988;103: 49–58. doi:10.1242/dev.103.1.49
- 1002 88. Eaton RC, Farley RD. Development of the mauthner neurons in embryos and larvae of the  
1003 zebrafish, *Brachydanio rerio*. *Copeia*. 1973;1973: 673. doi:10.2307/1443067
- 1004 89. Kimmel CB, Hatta K, Metcalfe WK. Early axonal contacts during development of an  
1005 identified dendrite in the brain of the zebrafish. *Neuron*. 1990;4: 535–545.  
1006 doi:10.1016/0896-6273(90)90111-r
- 1007 90. Kimmel CB, Sessions SK, Kimmel RJ. Morphogenesis and synaptogenesis of the zebrafish  
1008 Mauthner neuron. *J Comp Neurol*. 1981;198: 101–120. doi:10.1002/cne.901980110
- 1009 91. Tanimoto M, Ota Y, Horikawa K, Oda Y. Auditory input to CNS is acquired coincidentally  
1010 with development of inner ear after formation of functional afferent pathway in zebrafish. *J*  
1011 *Neurosci*. 2009;29: 2762–2767. doi:10.1523/JNEUROSCI.5530-08.2009
- 1012 92. Siomi MC, Siomi H, Sauer WH, Srinivasan S, Nussbaum RL, Dreyfuss G. FXR1, an  
1013 autosomal homolog of the fragile X mental retardation gene. *EMBO J*. 1995;14: 2401–  
1014 2408. doi:10.1002/j.1460-2075.1995.tb07237.x
- 1015 93. Zhang Y, O'Connor JP, Siomi MC, Srinivasan S, Dutra A, Nussbaum RL, et al. The fragile  
1016 X mental retardation syndrome protein interacts with novel homologs FXR1 and FXR2.  
1017 *EMBO J*. 1995;14: 5358–5366. doi:10.1002/j.1460-2075.1995.tb00220.x
- 1018 94. Bakker CE, de Diego Otero Y, Bontekoe C, Raghoe P, Luteijn T, Hoogeveen AT, et al.  
1019 Immunocytochemical and biochemical characterization of FMRP, FXR1P, and FXR2P in  
1020 the mouse. *Exp Cell Res*. 2000;258: 162–170. doi:10.1006/excr.2000.4932
- 1021 95. Agulhon C, Blanchet P, Kobetz A, Marchant D, Faucon N, Sarda P, et al. Expression of  
1022 FMR1, FXR1, and FXR2 genes in human prenatal tissues. *J Neuropathol Exp Neurol*.  
1023 1999;58: 867–880. doi:10.1097/00005072-199908000-00009
- 1024 96. Tucker B, Richards R, Lardelli M. Expression of three zebrafish orthologs of human FMR1-  
1025 related genes and their phylogenetic relationships. *Dev Genes Evol*. 2004;214: 567–574.  
1026 doi:10.1007/s00427-004-0438-9
- 1027 97. Coffee RL Jr, Tessier CR, Woodruff EA 3rd, Broadie K. Fragile X mental retardation protein  
1028 has a unique, evolutionarily conserved neuronal function not shared with FXR1P or  
1029 FXR2P. *Dis Model Mech*. 2010;3: 471–485. doi:10.1242/dmm.004598
- 1030 98. Boczkowska M, Rebowski G, Kast DJ, Dominguez R. Structural analysis of the transitional  
1031 state of Arp2/3 complex activation by two actin-bound WCAs. *Nat Commun*. 2014;5: 3308.  
1032 doi:10.1038/ncomms4308
- 1033 99. Lacoste AM, Schoppik D, Robson DN, Haesemeyer M, Portugues R, Li JM, et al. A  
1034 convergent and essential interneuron pathway for Mauthner-cell-mediated escapes. *Curr*  
1035 *Biol*. 2015;25: 1526–1534. doi:10.1016/j.cub.2015.04.025 [doi]

- 1036 100. Darnell JC, Van Driesche SJ, Zhang C, Hung KYS, Mele A, Fraser CE, et al. FMRP  
1037 stalls ribosomal translocation on mRNAs linked to synaptic function and autism. *Cell*.  
1038 2011;146: 247–261. doi:10.1016/j.cell.2011.06.013
- 1039 101. Möhrle D, Wang W, Whitehead SN, Schmid S. GABAB Receptor Agonist R-Baclofen  
1040 Reverses Altered Auditory Reactivity and Filtering in the *Cntnap2* Knock-Out Rat. *Front*  
1041 *Integr Neurosci*. 2021;15. doi:10.3389/fnint.2021.710593
- 1042 102. Waldmeier PC, Kaupmann K, Urwyler S. Roles of GABAB receptor subtypes in  
1043 presynaptic auto- and heteroreceptor function regulating GABA and glutamate release. *J*  
1044 *Neural Transm*. 2008;115: 1401–1411. doi:10.1007/s00702-008-0095-7
- 1045 103. Wu C, Sun D. GABA receptors in brain development, function, and injury. *Metab Brain*  
1046 *Dis*. 2015;30: 367–379. doi:10.1007/s11011-014-9560-1
- 1047 104. Tureček R, Melichar A, Králíková M, Hrušková B. The role of GABAB receptors in the  
1048 subcortical pathways of the mammalian auditory system. *Front Endocrinol* . 2023;14:  
1049 1195038. doi:10.3389/fendo.2023.1195038
- 1050 105. Berry-Kravis E, Hagerman R, Visootsak J, Budimirovic D, Kaufmann WE, Cherubini M,  
1051 et al. Arbaclofen in fragile X syndrome: results of phase 3 trials. *J Neurodev Disord*.  
1052 2017;9: 3. doi:10.1186/s11689-016-9181-6
- 1053 106. Veenstra-VanderWeele J, Cook EH, King BH, Zarevics P, Cherubini M, Walton-Bowen  
1054 K, et al. Arbaclofen in Children and Adolescents with Autism Spectrum Disorder: A  
1055 Randomized, Controlled, Phase 2 Trial. *Neuropsychopharmacology*. 2017;42: 1390–1398.  
1056 doi:10.1038/npp.2016.237
- 1057 107. Erickson CA, Veenstra-Vanderweele JM, Melmed RD, McCracken JT, Ginsberg LD,  
1058 Sikich L, et al. STX209 (arbaclofen) for autism spectrum disorders: an 8-week open-label  
1059 study. *J Autism Dev Disord*. 2014;44: 958–964. doi:10.1007/s10803-013-1963-z
- 1060 108. Mattson MP, Gleichmann M, Cheng A. Mitochondria in neuroplasticity and neurological  
1061 disorders. *Neuron*. 2008;60: 748–766. doi:10.1016/j.neuron.2008.10.010
- 1062 109. Smith GM, Gallo G. The role of mitochondria in axon development and regeneration.  
1063 *Dev Neurobiol*. 2018;78: 221–237. doi:10.1002/dneu.22546
- 1064 110. Safer D, Elzinga M, Nachmias VT. Thymosin beta 4 and Fx, an actin-sequestering  
1065 peptide, are indistinguishable. *J Biol Chem*. 1991;266: 4029–4032. Available:  
1066 <https://www.ncbi.nlm.nih.gov/pubmed/1999398>
- 1067 111. Yu FX, Lin SC, Morrison-Bogorad M, Atkinson MA, Yin HL. Thymosin beta 10 and  
1068 thymosin beta 4 are both actin monomer sequestering proteins. *J Biol Chem*. 1993;268:  
1069 502–509. doi:10.1016/s0021-9258(18)54179-x
- 1070 112. Cheng IH, Lin Y-C, Hwang E, Huang H-T, Chang W-H, Liu Y-L, et al. Collagen VI  
1071 protects against neuronal apoptosis elicited by ultraviolet irradiation via an  
1072 Akt/phosphatidylinositol 3-kinase signaling pathway. *Neuroscience*. 2011;183: 178–188.  
1073 doi:10.1016/j.neuroscience.2011.03.057



1074 113. Fox MA. Novel roles for collagens in wiring the vertebrate nervous system. *Curr Opin*  
1075 *Cell Biol.* 2008;20: 508–513. doi:10.1016/j.ceb.2008.05.003

1076

1077

## 1078 **Figure Legends**

### 1079 **Figure 1. Cyfip2 establishes the acoustic startle threshold through Rac1 and FMRP.**

1080 (A) Cyfip2 protein interacting domain diagram of wildtype (top) and mutant (bottom) Cyfip2  
1081 proteins. Black arrowheads indicate the positions of induced mutations in Cyfip2, eliminating the  
1082 Rac1- (C179R) or FMRP/eIF4E (K723E)-binding capacity of Cyfip2. (B) Cyfip2 actin regulatory  
1083 pathway wherein Cyfip2 (orange) upon stimulation by Rac1-GTP triggers WAVE1 activation,  
1084 Arp2/3-complex initiation and branched actin nucleation. (C) Cyfip2 translational repression  
1085 pathway in which Cyfip2, eIF4E (teal), and FMRP (pink) along with the poly-A binding protein  
1086 (PABP; gray), sequester neurodevelopmentally important mRNAs from being translated. (D)  
1087 Average startle frequency (%) after 10 trials at 13.6, 25.7, 29.2, 35.5, 39.6 and 53.6 dB for 5 dpf  
1088 *cyfip2* siblings (+/) and mutant (-/-) larvae heatshocked at 30 hpf for 40 minutes at 38°C. The  
1089 average startle frequency curve for *cyfip2* siblings (+/; open circles, dashed line), *cyfip2* mutants  
1090 (-/-; closed circles, solid line) and *cyfip2* mutants harboring the *Tg(hsp70:cyfip2-EGFP)+*  
1091 transgene (-/-; Tg+; closed circles, solid green line). (E) Sensitivity indices, calculated as the  
1092 area under the startle frequency curves, for 5 dpf *cyfip2* siblings and mutants, following a 40-  
1093 minute heatshock at 30 hpf to express either wildtype (Tg+; green), Rac1- ( $\Delta$ Rac1+; blue) or  
1094 FMRP/eIF4E- ( $\Delta$ FMRP+; pink) binding deficient versions of Cyfip2-EGFP. Comparisons were  
1095 made to both non-transgenic (Tg-) and non-heatshocked controls. All indices (mean  $\pm$  SD)  
1096 compared using a Kruskal-Wallis test with Dunn's multiple comparisons correction;  $p^{****} <$   
1097 0.0001. (F) Sensitivity indices for 5 dpf *cyfip2* sibling (+/) and mutant (-/-) larvae following 1-cell  
1098 stage injection with CRISPR-Cas9 and a single, scrambled guide RNA (gRNA) or dual gRNA

1099 cocktails targeting *fmr1*, *fxr1*, or *fxr2*. scrambled gRNA injected (white bar, closed circles); *fmr1*  
1100 gRNA injected (dark gray bar closed circles); *fxr1* gRNA injected (medium gray bar; closed  
1101 circles); *fxr2* gRNA injected (light gray bar, closed circles). Comparisons were made both within  
1102 genotype and between genotypes by condition. All indices (mean  $\pm$  SD) compared using an  
1103 Ordinary one-way ANOVA with Sidak's multiple comparisons correction;  $p^* < 0.05$ ;  $p^{**} < 0.01$ ;  
1104  $p^{****} < 0.0001$ .

1105

1106 **Figure 2. Cyfip2 acutely regulates branched actin polymerization and NMDARs to**  
1107 **establish the acoustic startle threshold.**

1108 (A) Sensitivity indices for 5 dpf *cyfip2* sibling (+/) and mutant (-/-) larvae, following a 40-minute  
1109 heatshock at 120 hpf (5 dpf) to express either wildtype (Tg+; green), Rac1- ( $\Delta$ Rac1+; blue) or  
1110 FMRP/eIF4E- ( $\Delta$ FMRP+; pink) binding deficient versions of Cyfip2-EGFP. Comparisons were  
1111 made to non-transgenic (Tg-), heatshocked sibling (+/) and mutant (-/-) controls. All indices  
1112 (mean  $\pm$  SD) compared using a Kruskal-Wallis test with Dunn's multiple comparisons correction;  
1113 p-values listed;  $p^{**} < 0.01$ ,  $p^{****} < 0.0001$ . (B) Sensitivity indices for 5 dpf *cyfip2* wildtype (+/+;  
1114 white bar) and heterozygous (+/-; gray bar) larvae, treated for 30 minutes on d5 with 5, 20 or 50  
1115  $\mu$ M CK-869. Comparisons were made both within genotype and within condition. All indices  
1116 (mean  $\pm$  SD) compared using a Kruskal-Wallis test with Dunn's multiple comparisons correction;  
1117  $p^* < 0.05$ ;  $p^{****} < 0.0001$ . (C) Sensitivity indices for 5 dpf Tüpfel longfin (TL) larvae treated for  
1118 30 minutes on d5 with the highest, non-lethal doses the formin antagonist (SMIFH2; 5  $\mu$ M),  
1119 PAK3 antagonist (IPA-3; 50  $\mu$ M) and ROCK antagonist (GSK429286; 100  $\mu$ M). Comparisons  
1120 were made between respective treatments and the DMSO controls. All indices (mean  $\pm$  SD)  
1121 were compared using a Kruskal-Wallis test with Dunn's multiple comparisons correction; All  
1122 comparisons made were non-significant (n.s.). (D) Sensitivity indices for 5 dpf *cyfip2* sibling (+/)

1123 and mutant (-/-) larvae, treated for 30 minutes on d5 with 100 or 500  $\mu$ M MK-801. Comparisons  
1124 were made both between genotypes within condition and between conditions by genotype. All  
1125 indices (mean  $\pm$  SD) were compared using an Ordinary one-way ANOVA with Tukey's multiple  
1126 comparisons correction.  $p^{**} < 0.01$ ;  $p^{***} < 0.001$ ;  $p^{****} < 0.0001$ .

1127

1128 **Figure 3. Loss of Cyfip2 causes widespread proteomic changes and GABAB receptor**  
1129 **signaling is critical for startle sensitivity.**

1130 (A) Bubble plots reporting the level of significance of the top 10 dysregulated proteins for both  
1131 *cyfip2* heterozygous (top) and mutant (bottom) groups compared to wildtype controls. The size  
1132 of the dot is proportional to the significance of the results while the color code represents the  
1133 log<sub>2</sub> fold change; top five upregulated (green), and top five downregulated (red) proteins are  
1134 shown. (B-C) Heat maps displaying the impacted canonical pathways (B) and diseases and  
1135 biological functions (C) from IPA functional analysis. The blue-colored gradient indicates the  
1136 degree of enrichment for the listed pathways or diseases/functions, as represented by the  $-\log$   
1137 of the P value for each pathway, disease and/or function. (D-E) Sensitivity indices for 5 dpf  
1138 *cyfip2* sibling (+/) and mutant (-/-) larvae, treated for 60 minutes prior to testing with muscimol  
1139 (D) or (E) baclofen. All indices (mean  $\pm$  SD) were compared using a one-way ANOVA with  
1140 Sidak's multiple comparisons correction.  $p^* < 0.05$ ,  $p^{**} < 0.01$ ;  $p^{***} < 0.001$ ;  $p^{****} < 0.0001$ .

1141

1142 **Tables**

Compound	Concentration ( $\mu$ M)	Effect By Genotype		
		<i>cyfip2</i> (+/+)	<i>cyfip2</i> (+/-)	<i>cyfip2</i> (-/-)
NPAA (Cl <sup>-</sup> -channel)	1	93.21% of Control, $p > 0.99$	110.21% of Control, $p < 0.99$	113.57% of Control, $p > 0.99$

antagonist)	5	140.11% of Control, p = 0.9785	137.32% of Control, p = 0.1385	140.29% of Control, p > 0.2787
	10	<b>234.14% of Control, p** = 0.0038</b>	<b>201.29% of Control, p**** &lt; 0.0001</b>	<b>155.06% of Control, p* = 0.0189</b>
MA (K+ channel/gap jxn. antagonist)	1	131.6% of Control, p > 0.99	11.87% of Control, p > 0.99	132.29% of Control, p = 0.5732
	5	137.24% of Control, p > 0.99	138.46% of Control, p = 0.0622	112.29% of Control, p > 0.99
	10	214.13% of Control, p = 0.0833	<b>169.81% of Control, p* = 0.0188</b>	<b>155.76% of Control, p* = 0.0288</b>
POBA (AAR/calmodulin antagonist)	1	102.9% of Control, p > 0.99	107.08% of Control, p > 0.99	101.04% of Control, p > 0.99
	10	136.17% of Control, p > 0.99	106.58% of Control, p > 0.99	99.01% of Control, p > 0.99
	50	<b>175.8% of Control, p* = 0.0123</b>		99.76% of Control, p > 0.99
ETAZ (PDE4 inhibitor)	1	141.79% of Control, p > 0.99	126.36% of Control, p > 0.99	121.74% of Control, p > 0.99
	10	168.6% of Control, p = 0.5472	<b>172.26% of Control, p* = 0.0137</b>	152.73% of Control, p = 0.3977
	50	<b>236.64% of Control, p** = 0.0029</b>	<b>179.99% of Control, p** = 0.0015</b>	<b>149.75% of Control, p* = 0.0105</b>
MK-801 (NMDAR antagonist)	100	120.19% of Control, p > 0.99		<b>145.93% of Control, p** = 0.0024</b>
	500	<b>212.69% of Control, p**** &lt; 0.0001</b>		<b>163.26% of Control, p*** = 0.0002</b>
BMS-204352 (K+ channel antagonist)	10	79.48% of Control, p = 0.4269		89.55% of Control, p > 0.99
	50	76.08% of Control, p = 0.6759		108.74% of Control, p > 0.99
NSC-23766 (Rac1 antagonist)	100	<b>49.14% of Control, p*** = 0.0002</b>		81.60% of Control, p > 0.99
	200	86.26% of Control, p > 0.99		105.28% of Control, p > 0.99

1143

1144 **Table 1. Cyfip2 may regulate NMDARs to control acoustic startle sensitivity.** Mean startle index  
1145 comparisons, listed as percentage (%) of the mean startle index of vehicle-treated controls by *cyfip2*  
1146 genotype and drug concentration, for larvae treated with compounds targeting the indicated pathways  
1147 [61] to increase acoustic startle sensitivity. All significant differences (p < 0.05) are listed (**bold**) for  
1148 comparisons using a Kruskal-Wallis test and Dunn's multiple comparisons correction. NPAA (*N*-  
1149 phenylanthranilic acid); MA (meclofenamic acid); POBA (phenoxybenzamine); ETAZ (etazolate).

1150

1151

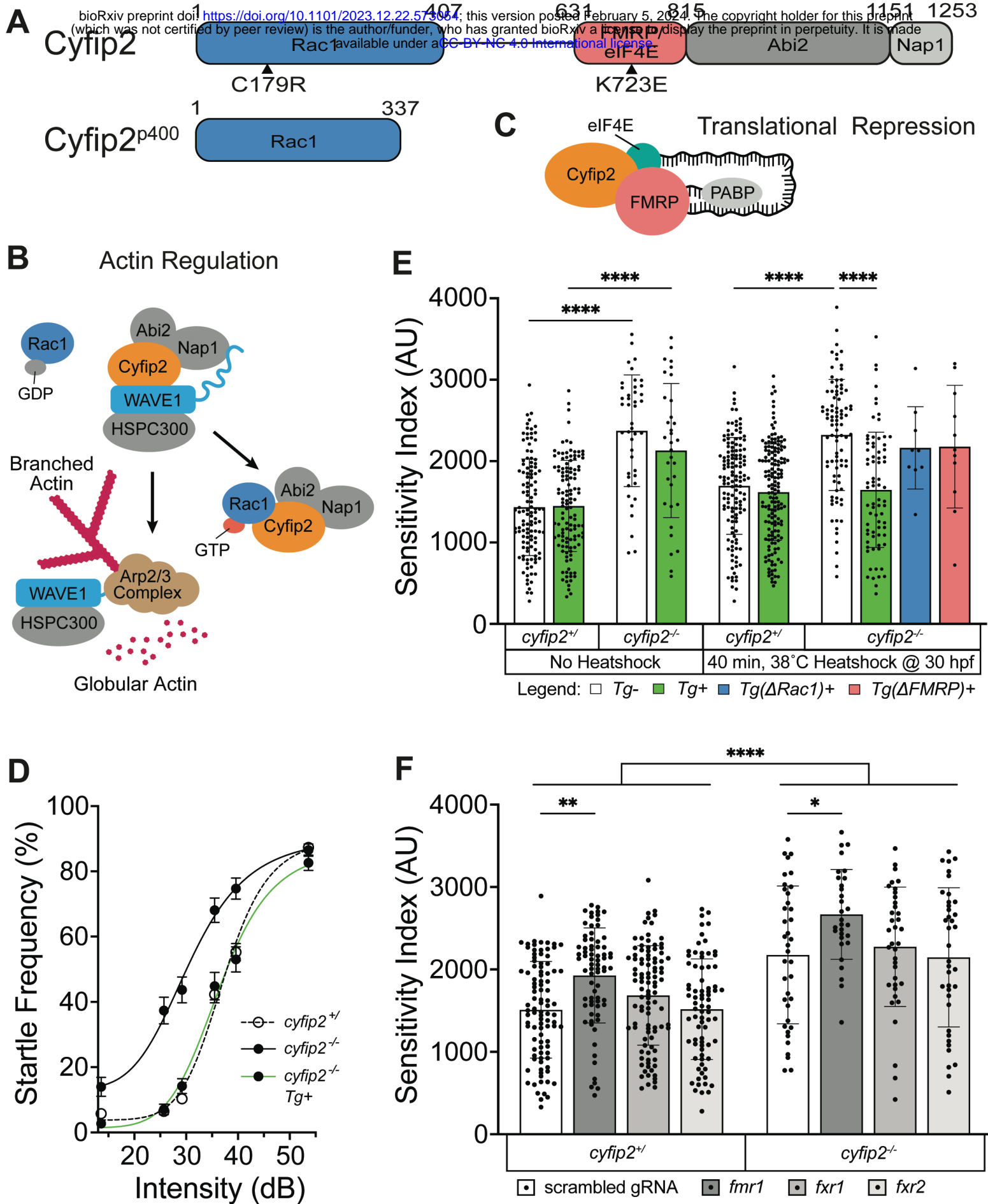


Figure 1 Deslauriers et al. 2023

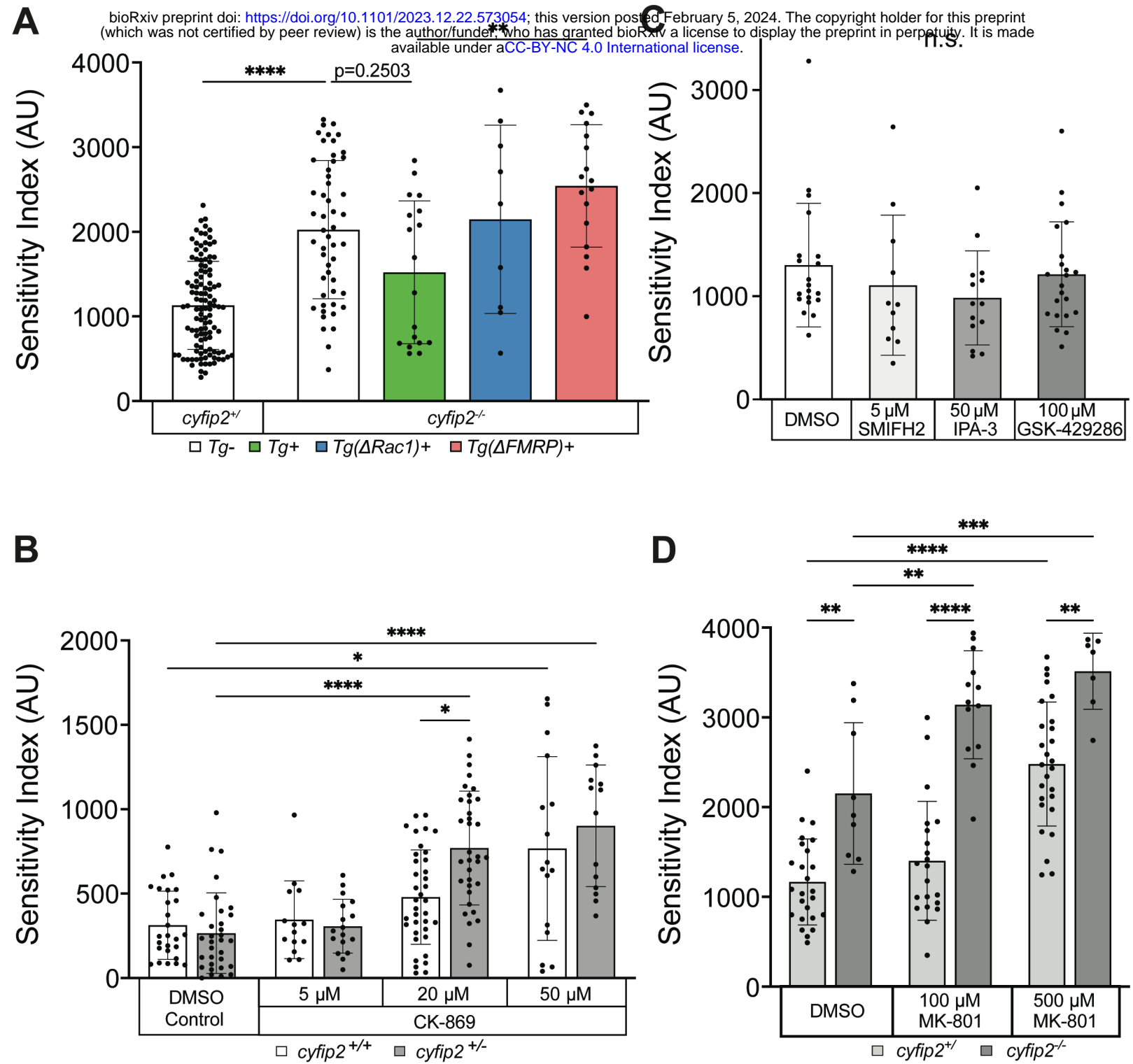


Figure 2 Deslauriers et al. 2023

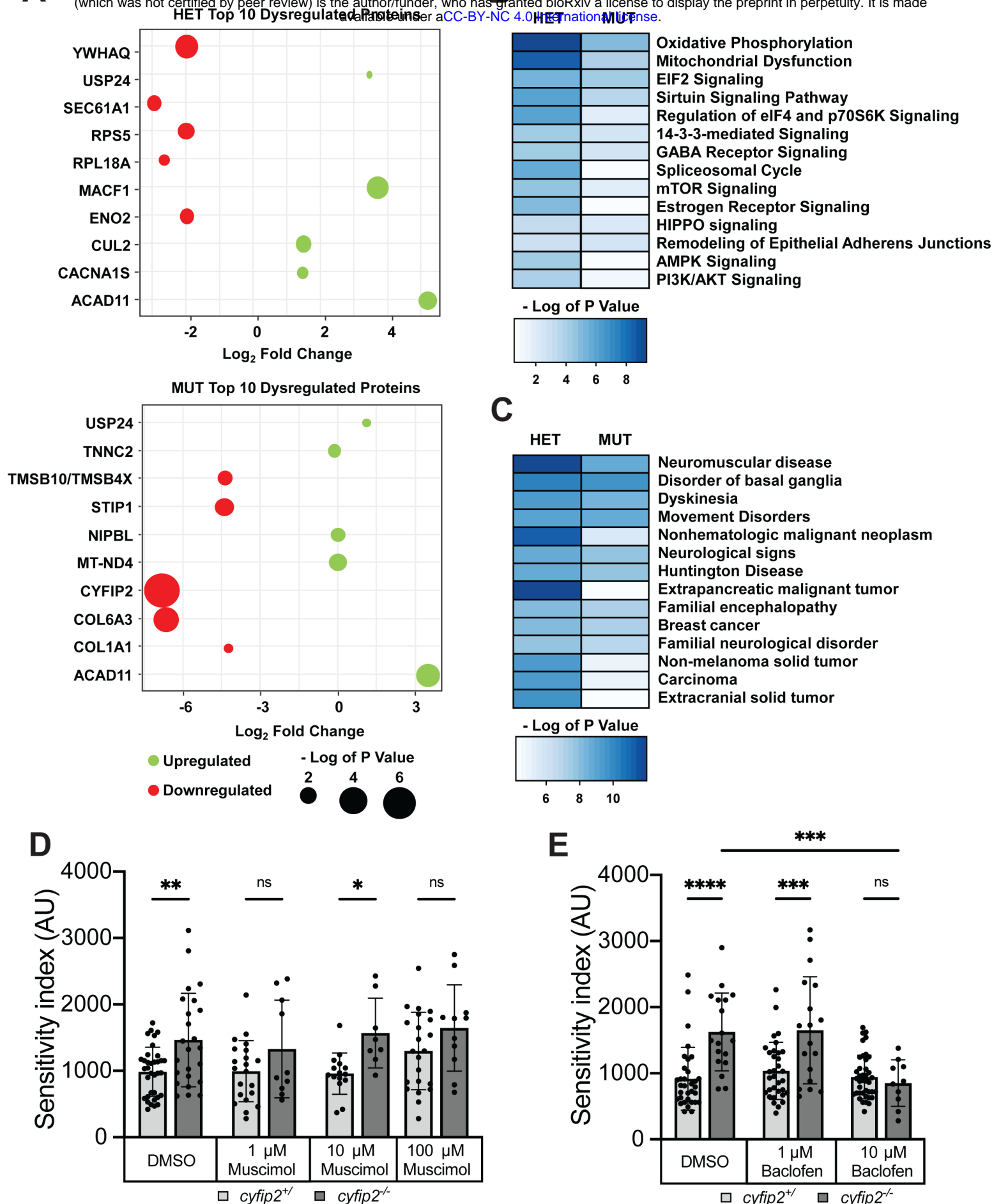


Figure 3 Deslauriers et al. 2023